Supporting Information Appendix

Pliocene reversal of late Neogene aridification

J.M.K. Sniderman, J. Woodhead, J. Hellstrom, G.J. Jordan, R.N. Drysdale, J.J. Tyler, N. Porch

SUPPLEMENTARY MATERIALS AND METHODS

Pollen analysis. We attempted to extract fossil pollen from 81 speleothems collected from 16 caves from the Western Australian portion of the Nullarbor Plain. Nullarbor speleothems and caves are essentially "fossil" features that appear to have been preserved by very slow rates of landscape change in a semi-arid landscape. Sample collection targeted fallen, well preserved speleothems in multiple caves. U-Pb dates of these speleothems (Table S3) ranged from late Miocene (8.19 Ma) to Middle Pleistocene (0.41 Ma), with an average age of 4.11 Ma.

Fossil pollen typically is present in speleothems in very low concentrations, so pollen processing techniques were developed to minimize contamination by modern pollen (1), but also to maximize recovery, to accommodate the highly variable organic matter content of the speleothems, and to remove a clay- to fine silt-sized mineral fraction present in many samples, which was resistant to cold HF and which can become electrostatically attracted to pollen grains, inhibiting their identification. Stalagmite and flowstone samples of 30-200 g mass were first cut on a diamond rock saw in order to remove any obviously porous material. All subsequent physical and chemical processes were carried out within a HEPA-filtered exhausting clean air cabinet in an ISO Class 7 clean room. Samples were washed repeatedly in distilled, deionized water, then etched in dilute (c. 0.5 M) HCl for 10 minutes to remove the outer few 100 μm of calcite, before washing repeatedly again in distilled water. Exotic *Lycopodium* spores (available in tablet form from Lund University, Sweden) were added to each sample in order to allow pollen concentrations to be estimated and to provide bulk for

centrifugation to act upon, before samples were dissolved in concentrated (12 M) HCl. The CaCl-rich solute was then diluted approximately four-fold with distilled water before centrifugation (3500 ppm for 3 minutes) to discard the solute component. Organic fractions were separated from residues using a Na-polytungstate heavy liquid (2) (empirical formula $Na_6O_{39}W_{12}$) made up to specific gravity 2.0. Those samples which yielded a substantial organic-rich supernatant were then immersed in 10% KOH at 80°C for 2-10 minutes. Following KOH, these samples, along with samples that yielded minimal organic supernatants, were dehydrated in 100% ethanol, then suspended in glycerol. Acetolysis was avoided in order to aid the identification of modern pollen contaminants (1).

The majority of speleothems contained ≤0.1 pollen grains g^{-1}, and, for most samples, no pollen was observed during complete scans of multiple glass slides representing ≥50% of the acid-resistant residue. Statistically meaningful quantities of pollen were recovered from 13 speleothems, mostly flowstones, from five caves (Table 1). We initially incorporated Carrera marble blanks into our processing protocol in order to monitor contamination rates, but it quickly became clear that the majority of samples in any processing batch contained no fossil pollen. The 68 (84% of the total) processed speleothems that contained no detectable fossil pollen thus served as analytical blanks which provided an indication of the rate of contamination by modern pollen. In total, six obviously modern (retaining cell contents and in perfect condition) pollen grains (of four taxa, *Ulmus*, *Alnus*, *Plantago lanceolata* type, and Poaceae) were observed in six of the 81 residues, implying an extremely low rate of contamination, relative to the total number of fossil pollen grains, commensurate with our use of HEPA-filtered workstations for this work. The first three modern pollen types represent exotic taxa present in urban environments near our Melbourne laboratory, and easily identified if encountered in a polleniferous sample. Poaceae includes many native species, so modern contaminant grains conceivably could be mistaken for fossils. However, the observed rate of pollen contamination implies that the proportions of fossil Poaceae, 0-

3.3% of the pollen sum, might in reality be as much as 0.2% lower, or 0-3.1% of the sum, a small difference that does not affect our interpretation of late Neogene vegetation and climate. In order to assess the possibility that speleothem pollen was derived from the host limestone, we processed samples of the Early-Mid Miocene Nullarbor Limestone. No pollen grains were observed in these residues.

Where possible, >100 pollen grains were counted from each sample. To achieve this in some cases several aliquots of speleothem were dissolved, up to 760 g, and in most cases the entire acid- and alkali-resistant residue was examined. Pollen was counted under compound light microscopy at 640 and 1600 x magnification on a Zeiss Axiolab A1 with N-Achroplan objectives, and photographed on a Zeiss Axioscope A1 compound microscope with EC Plan-Neofluar objectives. All identified pollen types were included in pollen sums. The size of pollen sums unavoidably varied by approximately one order of magnitude, which entailed large variability in confidence estimates of pollen percentages (3). We therefore computed 95% confidence intervals for observed pollen percentages (3, 4) in order to explicitly account for this variability. Deteriorated and unidentifiable grains were observed in low quantities, but generally pollen was either in acceptable to excellent condition, or absent.

Pollen and spore identifications were made by comparison with pollen reference collections and with published pollen atlases, including the Australasian Pollen and Spore Atlas (apsa.anu.edu.au). For taxonomic groups for which existing knowledge of pollen morphological diversity was poor, new modern pollen reference material was generated by sampling voucher specimens at the National Herbarium of Victoria (MEL), supported by new collections in the field. For *Banksia* (Proteaceae), which includes approximately 170 species, we took advantage of the availability of a nearly complete species level molecular phylogeny based on five chloroplast DNA regions (5-7) to map pollen morphological features observed under light microscopy onto a phylogenetic framework. Below, pollen

nomenclature follows Punt et al. (8) and updates at http://www.pollen.mtu.edu/glos-gtx/glos-int.htm.

Speleothem pollen taphonomy. Below, we briefly summarize current understanding of modes of pollen transport into caves, before considering the role of taphonomic processes in the transport and preservation of pollen in Nullarbor speleothems. Although rates of pollen deposition in caves are typically much less than in lake sediments, studies indicate that cave sediment pollen spectra are representative of the surrounding vegetation (9), and similar to the spectra found in nearby outdoor pollen traps and small lakes (9, 10). Pollen may be brought into caves within drip water, through airborne transport, by animals, or by streams (11). The status of drip waters as pollen sources is equivocal, with some studies finding substantial quantities of pollen in drip water (12), others finding very little or none (10, 11). Studies of airborne pollen transport and deposition within caves indicate that the quantities of deposited pollen decrease with distance into the cave (9, 10). Where pollen is transported into caves by animals, its impact on pollen spectra is expected to increase with cave depth, as airborne pollen fluxes decline (13, 14).

The Nullarbor Plain is a broad surface of low relief, with limited deformation of its horizontally oriented stratigraphy since its emergence from the sea during the mid-late Miocene (15). There are no known lithological sources of reworked pollen on the Nullarbor Plain other than the Nullarbor Limestone itself (which contained no pollen, see above). Speleothems were collected from caves at depths below surface of 10-20 m. Drip water flow paths are interpreted to be relatively simple through the overlying epikarst. Modern entrances to late Neogene Nullarbor caves are unlikely to have persisted in the landscape for more than a few 100 kyr, and are uninformative about the location of cave entrances at the time of speleothem growth during the late Neogene. Thus, we do not know the position of any speleothem with respect to cave openings at the time of its growth.

The acid-resistant residues of approximately 60% of the 81 processed speleothem samples contained only small amounts of quartz and/or other siliciclasts. The remaining ~40% included a silt- to clay-sized biogenic and mineral fraction comprising fungal spores, charcoal and heavy minerals, which we interpret as airborne dust. Of these, 13 samples included usable concentrations of pollen. The simplest interpretation of this pattern is that the 'clean' Nullarbor speleothems grew at times when their caves had no connection to the surface, while those containing biogenic/mineral dust fractions grew at times when their caves had one or more entrances open to the atmosphere, allowing dust to be introduced onto growing speleothem surfaces. Because the polleniferous samples represent a subset of samples containing biogenic and mineral dusts, we infer that pollen was not generally derived from drip waters, but from the atmosphere. This interpretation implies that, at least for Nullarbor caves, the presence of fossil pollen within speleothems depends both on a cave having had ≥1 entrances at the time of speleothem growth, and on other conditions at the speleothem surface having being favourable for pollen preservation. The nature of these conditions is unknown; speculatively, the first order condition may be the need for speleothem growth rate to be above some minimum threshold. It is currently difficult to test this assumption because late Neogene speleothem U-Pb 2σ age errors are of the order of 100 kyr. In addition to an airborne component, the surprisingly strong representation of some animal-pollinated taxa, such as *Geniostoma*, implies that animals (presumably insects, based on the modern bird and insect pollination ecology of the genus in New Zealand(16)) were a quantitatively important pollen source. Idiosyncratic, animal-derived pollen spectra may be expected in speleothems remote from entrances(10), but the presence of *Geniostoma* pollen in speleothems from three caves also may imply that the source species was a cave-entrance habitat specialist, which is perhaps consistent with the fire-free habitat of *Geniostoma* today in New Zealand, other Pacific islands, and in northeastern Australian rainforest.

Pollen identification and interpretation of pollen assemblages. The Nullarbor speleothem pollen record demonstrates a new approach for revealing the environmental history of currently arid or semi-arid regions, particularly where, as in Australia, late Neogene aridification (17) has inhibited the preservation of most non-vertebrate fossil materials over very large areas, and very limited tectonic activity has inhibited the accumulation of thick sequences of the fine-grained lacustrine and fluvial sediments that typically preserve fossil pollen (18). Consequently there are very few late Neogene fossil pollen or paleobotanical records in Australia remote from the well-watered continental margins (18). It is thus not surprising that the late Miocene and Pliocene Nullarbor pollen archive indicates the presence of plant taxa (e.g. *Doryanthes* and *Geniostoma*) that have not been recorded previously in the late Cenozoic Australian plant fossil record. Carbonate lithologies typically generate neutral to alkaline soils that in many regions differ significantly in their characteristics for plant growth compared to soils developed on silicic lithologies, so speleothem fossil pollen assemblages may include taxa that are absent from or rare in pollen records from silicic landscapes. For example, in the British Late Quaternary Murton et al (19) found that speleothem fossil pollen assemblages reflected the flora of a limestone region which was not well documented by pollen records from silicic landscapes. In addition, speleothem pollen assemblages from the very extensive and flat Nullarbor Plain are very likely to avoid the pervasive bias towards wetland plant communities that routinely affects fossil pollen assemblages from lakes and wetlands (20). In examining Nullarbor fossil pollen assemblages, we encountered three distinctive pollen types (*Geniostoma*, *Doryanthes*, and *Banksia*/*Phanerostomata* eastern clade) which do not appear to be documented previously in the Australasian Cenozoic or Quaternary palynological literature. We undertook new analyses to identify these pollen types.

The Nullarbor pollen record is robust because each pollen sample is derived from a separate radiometrically dated speleothem, with ages directly traceable to the EarthTime

initiative reference materials (www.earth-time.org). This distinguishes it from other terrestrial records of Southern Hemisphere Pliocene vegetation (21). The record also contrasts with marine pollen records, which in some cases have broadly reliable chronologies based on biostratigraphy and/or magnetostratigraphy, but which typically integrate pollen from sub-continental regions. For example, a Late Quaternary marine sediment core taken 115 km offshore of North Island, New Zealand, integrated pollen derived from 400-500 km of coastline, conflating the vegetation histories of cool- and warm-temperate forest biomes (22). By contrast, speleothems preserve pollen derived from local to regional vegetation (11), implying pollen source radii of <10 km. Differences between the pollen assemblages of coeval speleothems from the five Nullarbor caves, with a mean inter-cave distance of ~25 km (range 7-60 km), may therefore be explained partly by vegetation patchiness or by other poorly understood taphonomic processes, especially given that some pollen types which are found inconsistently (*Banksia*, Doryanthaceae) are animal-pollinated. However, the pollen spectra of Pliocene samples younger than c. 4.9 Ma, derived from four different caves, are all consistently dominated by *Eucalyptus*, implying that the record as a whole is representative of regional vegetation. Moreover, the shallow climatic and vegetation gradients that characterize the Nullarbor Plain today (23) are determined by the region's limited topographic relief (Fig S1*B*), which has changed little during the late Neogene (24). We therefore conclude that the patterns of vegetation and climate change revealed in the speleothem record are representative of Pliocene environments across central southern Australia.

Paleoprecipitation estimates. We estimated mean annual precipitation for the 13 pollen assemblages, based on a probabilistic extension of the mutual climatic range approach (25-28). We interpreted the affinities of the Nullarbor fossil pollen types to extant plant taxa or clades (see Supplementary Information), and then gathered modern occurrence data for these taxa or clades. We drew on publically accessible online databases of plant occurrence data,

for Australia, New Zealand, and globally. For Australia, we acquired data from the Atlas of Living Australia (ALA) (www.ala.org.au), NatureMap (29), the Australian Ecological Knowledge and Observation System maintained by the Terrestrial Ecosystem Research Network at the University of Adelaide (http://www.tern.org.au); The New Zealand National Vegetation Survey Databank maintained by Landcare Research, New Zealand (https://nvs.landcareresearch.co.nz); and the Global Biodiversity Information Facility (www.gbif.org). These databases contain large quantities of data, the great majority of which is presence only (PO) data. PO data demonstrates the presence of a taxon at a particular time and place but does not necessarily provide a reliable indication of locations where that taxon is absent (30).

For species distribution modeling (31), the limitation of PO data is that they cannot provide a reliable estimate of species prevalence, or the proportion of sites in the region of interest in which a species is present (32), largely because the opportunistic and selective nature of species occurrence records means that PO data suffer from strong sampling biases (for example, there are more records near cities, and along roads within remote regions). It is thus difficult to generate quantitative estimates of the probability of occurrence of a species or taxon from PO data, as a function of selected climate (or other environmental) parameters (33, 34). We therefore restricted our data search to systematic survey data, in which multiple species records from a single site include (at least nominally) all plant taxa that were present at the time of survey. By implication, it can be assumed that taxa not recorded within a survey were actually absent from the site when it was surveyed. For interpretation of the probability of occurrence of a taxon as a function of one or more environmental variables, these presence/absence data are less influenced by sampling biases because densely sampled regions harbor more presences but also more absences (35). While absences may be unreliable for taxa that are rare or difficult to detect (36), our taxa of interest are either perennial shrub to tree sized plants, or, in the case of monocotyledonous *Doryanthes*, a

highly distinctive giant rosette plant. It is unlikely that any of the taxa would be missed in even a cursory vegetation survey, unless locally very rare (but in which case it is unlikely they would have contributed to a pollen flora).

We downloaded vascular plant data for Australia, using as filters the following exclusions: exotic species, records of cultivated specimens, records prior to 1970, spatially suspect records, records explicitly within non-native vegetation, and records with taxon identification issues. We recovered plant surveys from two sources: datasets of explicit regional to State-level plant surveys, included within online databases; and our own inferred surveys, which were extracted by filtering species occurrence data according to the following rules: groups of species occurrences were treated as "surveys" where they shared a species name, latitude and longitude (in some cases after smoothing to three significant digits), collector name, locality and site name (where supplied), and collection date (smoothed to one week to account for surveys that were conducted over several days). From the resulting sets of records, we excluded sets consisting of small numbers of species, typically less than ten, which we considered were unlikely to represent complete surveys of field quadrats or survey areas. We arbitrarily excluded sets of records containing more than 200 species, on the assumption that these sets most likely represented artificially precise geocoding of observation records during extensive plant collecting within an area substantially larger than a field plant survey (typically up to c. 0.1 ha). The resulting filtered dataset consisted of more than 101,000 sets of Australian plant species, herein referred to as "surveys". We scored the survey dataset for presence/absence of our target taxa: Gyrostemoanceae; *Glischrocaryon* and *Haloragodendron* (indistinguishable palynologically, and possibly phylogenetically: *Haloragodendron* is paraphyletic with respect to *Glischrocaryon*, according to the phylogeny of Chen et al. (37); Casuarinaceae; *Corymbia*/*Angophora* (indistinguishable palynologically); *Eucalyptus*; *Banksia* clades /*Cryptostomata*, /*Phanerostomata* 1, 2E and 2SW; Ericaceae; Asteraceae Cichorioideae; *Doryanthes*.

Two clades (*Geniostoma* and Chenopodiaceae) required special treatment because the survey data described above were inadequate for these taxa. *Geniostoma* occurs in only two of the >101,000 Australian surveys (Fig. S2*M*). We therefore acquired survey records of *Geniostoma* from two landmasses in which it is a widespread and common genus: for New Zealand, we recovered c. 5500 vascular plant surveys from The New Zealand National Vegetation Survey Databank (Fig. S2*K*, *L*). However, the New Zealand climate space is truncated at mean annual temperatures above c. 16°C, so we generated 'pseudo-surveys' from detailed distribution data of Hawaiian *Geniostoma* spp (as *Labordia*), from Price et al. (38). Price et al. provide high-resolution maps of modelled historical distributions of species of *Labordia*, based on all available species records. We created a 1.5' grid (approximately 7.3 km^2) for the Hawaiian archipelago, and scored the centroid of each cell for presence or absence of *Labordia* according to the maps described above. The result was therefore equivalent to presence absence point data with matching climate data. The resulting pseudo-surveys (Fig. S7*B*) were then combined with the New Zealand data and analyzed using the same methods as for all taxa except Chenopdiaceae. For Chenopodiaceae, recent taxonomic changes (the transfer of chenopods to Amaranthaceae (39)) resulted in an error within ALA in which species belonging to the former Chenopodiaceae had been transferred out of that family, but not yet transferred into Amaranthaceae. As a result, no records for this clade were returned from ALA searches based on locations. We therefore modelled climate parameters for the former Chenopodiaceae based on modern pollen-vegetation relationships, requiring a different analytical approach (see below).

Mean annual precipitation was reconstructed based on probability distribution functions inferred using generalized additive modeling (GAM), implemented using the gam function in the mgcv package (40) in R (41). The approach for all clades except Chenopodiaceae was as follows: for each survey location we used an SRTM-derived 1 second digital elevation model to infer site altitude, and then used this data combined with

261 latitude and longitude to estimate mean annual precipitation at each survey location with
262 ANUCLIM (42). For each clade we created a GAM with mean annual precipitation as the
263 independent variable and presence/absence of the clade as the dependent variable, assuming
264 a binomial distribution and a cubic regression spline. We then predicted the score for
265 approximately 19,000 points along the range of the mean annual precipitation, and inferred
266 that this score represented the probability of occurrence of that clade at that mean annual
267 precipitation.

268 The probability function for the former Chenopodiaceae was assembled in a different
269 way. The family is well represented in surface and pre-European wetland pollen samples,
270 which can be used as modern analogues of fossil assemblages. We made the uniformitarian
271 assumption that the relationship between the abundance of Chenopodiaceae pollen in surface
272 and pre-European wetland samples and climate can be used to predict past climates from the
273 abundance of fossil Chenopodiaceae pollen. We used surface and pre-European pollen
274 sample data documented in the southeast Australian pollen database (43) supplemented by
275 modern pollen trap and late Holocene samples from southwestern Australia (44, 45). A
276 Gaussian GAM based on a cubic regression spline was created with the abundance of
277 Chenopodiaceae pollen in 159 samples as the independent variable and the log of mean
278 annual precipitation for the collection site of each sample as the dependent variable. The log
279 transformation ensured that the residuals were approximately normally distributed, which
280 allowed us to infer the probability distribution of the predicted mean annual precipitation for
281 a given abundance of Chenopodiaceae as the inverse Z distribution (approximated as the t-
282 distribution with high degrees of freedom).

283 To calculate the joint probability function for each of the 13 Nullarbor fossil pollen
284 samples relative to mean annual precipitation we multiplied the individual relative
285 probability functions of each clade present within that pollen sample, then scaled the
286 resulting function so that the cumulative total was 1. The data were truncated at ≤2500mm

mean annual precipitation because survey data from ALA are very sparse for climates wetter than this (representing less than 0.2% of all surveys) and the maximum values for most clades within each pollen sample were well below this number.

Geochronology. The analytical methods employed in this study follow closely those published previously by Woodhead et al. (46, 47). Multiple aliquots, typically weighing ~50 mg, were removed from each speleothem sample using a dental drill. The pieces of calcite removed in this way were then placed into pre-cleaned disposable polyethylene cups and moved to a multiple-HEPA filtered clean room environment. Samples were briefly leached two times in very dilute (~0.01 M) three-times teflon distilled HCl, with each cycle lasting around one minute, and then repeatedly washed in ultra-pure water before being dried in a HEPA filtered laminar flow hood. This step is critical to the elimination of Pb contaminants resulting from sample handling which can easily dominate the Pb budget of the entire sample unless removed.

Individual samples were weighed into pre-cleaned teflon beakers and treated with sufficient 6N HCl to ensure complete dissolution. A mixed ^{233}U-^{205}Pb tracer, calibrated against EarthTime (http://www.earth-time.org) reference solutions, was then weighed into the vials and each one sealed and refluxed on the hotplate for several hours to ensure complete sample-spike equilibration. Samples were then dried down and taken up in 0.6N HBr for Pb separation using a single pass over AG 1X-8 anion exchange resin. The eluate from the first column (U + matrix) was subsequently processed through the same column now emptied of AG 1X-8 and refilled with Eichrom TRU ion-specific resin, to separate U. Pb blanks were typically 10±5pg and were corrected for. U blanks were insignificant relative to the amounts of U being processed.

Isotope ratios were determined on a Nu Plasma MC-ICPMS using a DSN-100 desolvation unit and MicroMist glass nebulizer, operating in the range 50-100 µl/min uptake. Instrumental mass bias effects were monitored and corrected using NIST SRM 981 reference

material in the case of Pb, and the sample's internal $^{238}U/^{235}U$ ratio (=137.88) in the case of U. Instrument data files were processed initially using an in-house designed importer, operating within the Iolite environment (48) which considers all data and reference material analyses obtained throughout a particular analytical session and permits a variety of corrections for instrumental mass bias and drift. The resulting data, now corrected for instrumental effects, were then blank corrected and isotope-dilution calculations performed using the Schmitz and Schoene software (49).

$^{238}U/^{206}Pb$-$^{207}Pb/^{206}Pb$ isochron regressions were calculated using 'Isoplot Ex'(50) and are labeled either 'Model 1' or 'Model 2', distinguished by MSWD less than or greater than 2.5 respectively (Table S3). In the former it is assumed that the assigned analytical errors are the only source of data scatter and points are therefore weighted according to the inverse square of these uncertainties. In situations where the software detects a low probability of fit based upon assigned errors alone (i.e. there is likely additional geological scatter) a so-called 'Model 2' fit is employed which instead assigns equal weights and zero error-correlations to each point. From a philosophical standpoint there are many reasons to move away from such 'stepwise' changes in uncertainty handling and some attempts have been made by the geochronology community to move in this direction [e.g. ref (51)]. As yet, however, these robust statistical methods are yet to be implemented for the U-Pb system and so the traditional approach (and that invoked by Isoplot Ex) is employed in this study. Isochron ages were calculated using in-house software using the intersection of isochrons with an appropriate disequilibrium concordia, with decay constants from refs [(52, 53)], and assuming negligible initial ^{230}Th ($^{230}Th/^{232}Th$ activity ratios are typically in excess of 5,000 but range up to ~50,000 (46). Any inaccuracies in final U-Pb age determinations caused by the assumption of zero ^{230}Th only amount to ~10ka maximum and thus have minimal impact on the final uncertainty budget. There is no independent means of assessing the likely $^{234}U/^{238}U$ initial activity ratios of Nullarbor cave drip waters and thus it is impossible to

make a robust correction for initial U-isotope disequilibrium effects. We therefore impose a realistic (hence necessarily broad) range in initial activity ratio of 1±0.3 during calculation of disequilibrium-corrected ages. This is based upon measurement of 17 Pleistocene Nullarbor speleothems for which measurable disequilibrium values can be detected. These provide a total range in $^{234}U/^{238}U_{initial}$ from 0.7 to 1.2 (46, 54). For all samples this results in an increase in age of only ~100 ka, within uncertainty of the uncorrected age.

Iterative age modeling. Each of our 13 pollen samples is derived from a separate speleothem. We therefore could not use stratigraphic superposition to evaluate their relative ages, but relied purely on the U-Pb age determination for each speleothem to build an age model for the pollen record. However, several speleothems have U-Pb ages with overlapping 2σ errors (Fig. 2; Table 1, Table S3). For any two speleothems with overlapping age errors, there is a finite probability that their true chronological sequence differs from that indicated by their median age estimates, and the closer together that they are with respect to their age uncertainties the more likely this is. We modeled these probabilities using a Monte Carlo procedure in which we iteratively sampled the Gaussian age distributions of each speleothem, repeating the process 100,000 times to develop a composite probability distribution which we summarize in terms of its median, lower and upper 1- and 2σ values. Simulated ages which did not fall within 2σ of any of the input age determinations were deleted, giving the effect of gaps in the simulated record where age determinations are separated by >2σ.

We undertook two Monte Carlo simulations. First, in order to model the temporal evolution of Nullarbor vegetation, a Monte Carlo procedure sampled the Gaussian probability distributions of each age determination as described above while simultaneously sampling the probability distribution of the observed pollen percentages, which follow a binomial distribution (4). Following Mosimann (4), we estimated a 95% confidence interval

for p, the true proportion of pollen type X, from $\hat{p} = x/n$, the number of grains of pollen type X observed within a pollen sum of n grains (eqn 1).

$$p_{0.95} = \frac{\hat{p} + \left[(1.96)^2/(2n)\right] \pm (1.96) + \sqrt{\left[\hat{p}(1-\hat{p})/n\right] + \left[(1.96)^2/(4n^2)\right]}}{1 + \left[(1.96)^2/n\right]} \quad (1)$$

By explicitly modeling how confidence in observed pollen percentages varies between samples with different pollen counts, this approach permitted us to include samples with highly variable pollen recovery, rather than simply discarding samples with relatively low yield on the basis that they fail to satisfy a minimum pollen count threshold. However, Mosimann's interval estimator assumes that confidence in any observation where $\hat{p} = 0$ is simply a function of n, that is, all zeroes are simply 'sampling' zeroes (55). Given the ~5 Myr span of the Nullarbor pollen record, encompassing three phylogenetically and climatically distinct biomes (late Miocene-earliest Pliocene, Early Pliocene, Mid Pleistocene), we preferred to risk making type II errors (treat source plants of unobserved pollen types as absent though they may in fact have been present) than type I errors (treat source plants of unobserved pollen types as present though they may in fact have been truly absent). We therefore treated zero percentage values as 'structural' or 'true' zeroes (55, 56), unless the 2σ age of their host speleothem fell within the 2σ age of another speleothem in the record that did show a non-zero count for that taxon.

Second, in order to model the temporal evolution of estimated Nullarbor mean annual precipitation, a Monte Carlo procedure sampled the Gaussian probability distributions of each age determination while simultaneously sampling from the empirical GAM-derived probability distributions (Fig. S4) of MAP for each of the 13 pollen assemblages.

For both Monte Carlo simulations, the resulting probability cloud was binned into a two-dimensional histogram of 500 by 500 bins. A cumulative probability curve was compiled for

388 each time slice of the histogram that lies within 2σ of an age determination, from which y-
389 values were determined for the median, and for corresponding upper- and lower-95%
390 confidence intervals.
391
392 **Time series analysis.** We located significant change points (57) in the mean of time series
393 using the cpt.mean function in the changepoint package (58) in R (41). We used the exact
394 method 'Pruned exact linear time' (59), with a manual penalty of $2\times\log(n)$, but change point
395 positions were identical using other methods. Prior to change point analysis, we resampled
396 the 2.6-7 Ma interval of the benthic $\delta^{18}O$ record of Zachos et al. (60) at a resolution of
397 0.00126 Ma (the mean sampling interval of the original data over this interval). We
398 recalculated the age models of the ODP 1095 and ODP 1165 records to align their control
399 points with the 2012 geomagnetic polarity time scale (61).
400 **Evaluation of the ages of published Southern Hemisphere vegetation records.** We
401 critically reviewed the quality of the age control of all Southern Hemisphere records
402 interpreted by Salzmann et al. (21, 62) as evidence for Late Pliocene (the Piacenzian epoch)
403 vegetation. We assigned conservative age estimates to each record (Table S1), defined in
404 relation to the strength of age control. Thus we separated the purported Late Pliocene records
405 into three broad categories based on decreasing geochronological accuracy and precision: (i)
406 records in which purported ages are based on dated pyroclastics and/or magnetostratigraphy
407 of long continuous sedimentary sections; (ii) records derived from marine sediments in
408 which purported ages are based on biostratigraphic comparison of globally distributed
409 marine faunas; (iii) records derived from terrestrial sediments in which purported ages are
410 based on regional biostratigraphic comparison of terrestrial fossil faunas or floras. We refer
411 to biostratigraphic comparisons as 'formal' when the basis for comparison is a published
412 biostratigraphic scheme provided with age control through approaches (i) and/or (ii); and
413 'informal' when the basis for the comparison appears to be unpublished, unorganized, and/or

414 removed by several steps from radiometric dates and/or from sedimentary sections supplied
415 with long, continuous magnetic polarity records. Where applicable, we estimated the
416 offshore distance of marine sediment records, as an approximate guide to the size of land
417 area that their pollen assemblages likely integrate.

418 We assigned very broad age ranges to most of the Australian vegetation records (Fig.
419 1, Table S1) because their published age determinations generally rely on relatively far-field
420 comparisons with the offshore Gippsland (18, 63, 64) or marginal marine Murray Basin (65,
421 66) palynostratigraphies. While these are formal biostratigraphic schemes, their age control
422 is in turn based largely on global comparisons of the first- and last appearance datums (FADs
423 and LADs) of marine faunas. The timing of some of these events exhibit interbasin- and
424 interhemispheric lags of epoch or sub-epoch scale (67). For example, the FADs of the
425 biostratigraphically-important foraminifera *Globorotalia truncatulinoides* in the South
426 Pacific (2.58 Ma) (68) and the South Atlantic (1.93 Ma) (68, 69) differ by 650 kyr, a lag
427 which essentially straddles the entire Piacenzian epoch. Even where planktic foraminifera
428 FADs are globally closely synchronous (68), dates recovered from the paleoceanographic
429 literature may be based on geomagnetic polarity timescales that are now obsolete.

430 The resulting uncertainties can be illustrated by Hapuku-1, the only long, late Neogene
431 pollen record derived directly within Gippsland Basin marine sediments. The two published
432 versions of the Hapuku-1 chronology (18, 70) differ in their placement of the Early/Late
433 Pliocene boundary by c. 300-400 m of sediment depth. Moreover, four Pliocene and Early
434 Pleistocene FADs (of *Globorotalia puncticulata*, *G. inflata*, *G. tosaensis* and *G.*
435 *truncatulinoides*) that form the basis for the most recently erected chronology (70) are out of
436 sequence, according to the most recent iteration of the Geological Time Scale (68). These
437 observations are consistent with Macphail's (18) conclusion with regard to southern
438 Australian Pliocene pollen records, that "it is by no means certain that all terrestrial
439 assemblages claimed to be Pliocene are correctly dated. This includes the widely cited

440 palynofloras from the Lachlan Valley (New South Wales)…(and)…Butchers Creek (NE
441 Queensland)" … Palynostratigraphic criteria developed for the Gippsland and Murray
442 Basins…confirm that the first two sites are unlikely to be older than Late Miocene or
443 younger than earliest Late Pliocene" (p. 429). An additional problem with dating terrestrial
444 vegetation records by comparison with marine sediment stratigraphies is the possibility of
445 diachronous timing of changes in vegetation between coastal lowlands and upland montane
446 regions. For example, an independently dated ~300 kyr long pollen record from upland
447 southeastern Australia (71) demonstrated the persistence until c. 1.5 Ma, during the Early
448 Pleistocene, of several mesic taxa which in offshore marine sediments disappeared much
449 earlier, during the Late Miocene or Pliocene (e.g. the angiosperm *Ilex* [*Ilexpollenites*
450 *anguloclavatus*], and the fern *Lophosoria* [*Cyatheacidites annulatus*]). Therefore, we cannot
451 exclude the possibility that published palynofloras considered "Pliocene", primarily on the
452 grounds that they include regionally to continentally extinct taxa, may be as young as Early
453 Pleistocene.

454 For other landmasses, we re-assessed the age ranges of purported Late Pliocene records
455 primarily by consulting the source publications. We assigned broad age ranges to records for
456 which published ages were determined by (typically more or less informal) biostratigraphic
457 comparisons. We took a skeptical view of the value of vegetation records based solely on
458 vertebrate fossil assemblages or on geomorphic and sedimentological evidence, regardless of
459 the quality of their age control. We consider that such records are unlikely to make
460 unambiguous contributions to knowledge of Pliocene vegetation.

461

462 **Identification of fossils.**

463 ***Banksia* (Proteaceae)**

464 *Pollen of extant species*

The Pliocene Nullarbor pollen assemblages included a range of diporate Proteaceae morphotypes comparable to *Banksia+Dryandra* (5, 72). In order to assess the taxonomic affinities of these fossils, we examined the pollen morphology of representatives of monophyletic species groups identified by chloroplast phylogenies of *Banksia* s.l. (incorporating *Dryandra* (5, 6)). We examined nine species within *Banksia*/*Cryptostomata* (using the clademark convention of Baum et al. (73); herein, clade C), and 18 species within *Banksia*/*Phanerostomata* (herein, clade P; Fig. S5). We looked for both categorical and continuously varying pollen morphological characters that correspond to monophyletic groups, to provide a basis for objectively assigning fossil grains to infrageneric clades within *Banksia*. Pollen measurements were made on digital photomicrograph images in Adobe Illustrator, using the Astute Graphics Vector Scribe Dynamic Measure tool. Where pollen grains were crescent-shaped, as in some species of clade C, equatorial axes were measured along arcs parallel to the grain outline and extending between the pores. The length of the pollen equatorial axes were significantly different between clades C and P (clade C, $n = 41$, $\bar{x} = 59.8$ µm; clade P, $n = 134$, $\bar{x} = 34.1$ µm, $p = 0.000$, Table S2, Fig. S5*A*, *B*). Within our data set, overlap in the length of the equatorial axis between the two clades is minimal: the length of the equatorial axis of the smallest observed pollen grain in clade C, 44.3µm, represents the 98.3 percentile of equatorial axis lengths observed in clade P grains.

Within clade P, a subclade confined to southwestern Australia which we refer to as P1 (Table S2, Figs S2*H*, S5*C*, *D*) is characterized by two pollen morphological features that distinguish it from the remainder of clade P, which we refer to as clade P2. These features of clade P1 include a distinctly rugulate exine sculpture (Fig. S6*X*); and a narrow internal pore diameter, relative to grain size (Fig. S5*C*, *D*). Within clade P1 we observed one anomalous species, *B. grandis*, which has psilate, rather than rugulate pollen, and much larger pores relative to the length of its polar axis. Possible explanations for this anomaly include (i) incorrect phylogenetic placement of *B. grandis* in clade P1; (ii) the pollen morphological

features of *B. grandis* may reflect a history of reticulate evolution involving species outside of clade P1; or (iii) pollen morphological features of *B*. *grandis* may represent an autapomorphy for the species or for a small group of species within clade P1. However, *B. grandis*, with a polar axis length of 33-38 μm, could not be mistaken for a member of clade P2, because the largest observed specimen in clade P2 had a polar axis of 30.2 μm. Within clade P2, 30 μm represents the 99.4 percentile of our polar axis length observations (Fig. S5*D*). Therefore, pollen of P1 is unlikely to be mistaken for pollen of P2, because the former is typically distinctly rugulate; or if not rugulate, has pollen which is larger than pollen of P1.

Clade P2 separates into two clades, which we refer to as clades P2SW and P2E, that are geographically confined, respectively, to southwestern Australian and to eastern and northern Australia (Fig. S2*G*). Pollen grains of clade P2SW are typically barrel-shaped in equatorial view, with a conspicuously biconvex amb, (Fig. S6*V*, *W*). By comparison, the outline of pollen grains of clade P2E are typically linear or plano-convex (Fig. S6*M*-*O*). We measured the mean radius of curvature (average of both sides of the grain) of the amb of seven species (48 spms) in clade P2E, and of six species (49 spms) in clade P2SW, and normalized the radius of curvature to the length of the polar axis. The resulting ratio of the radius of curvature to the length of the polar axis was significantly different between clades P2SW and P2E (clade P2SW, n=49, $\bar{x}$ =1.02; clade P2E, n=48, $\bar{x}$ = 2.64, p = 0.000, Table S2, Fig. S5*E*, *F*). However, there is some overlap between the two clades: the minimum value of the ratio in the clade P2E dataset, 1.317, represents the 86 percentile of the clade P2SW dataset (Fig. S5*F*). That is, our data suggest that there is nominally a 14% chance of mistaking a dispersed pollen grain of clade P2SW for a pollen grain of clade P2E.

We used these categorical (rugulate vs. non-rugulate exine sculpture) and continuous (equatorial axis length; ratio of polar axis length to internal pore diameter; ratio of the radius of curvature to the polar axis length) variables to develop a hierarchical classification of the modern acetolysed pollen of *Banksia*. We emphasize the separation of lineages within

/*Phanerostomata* because grains consistent with the latter numerically dominate our fossil assemblages:

Banksia:

1a. Equatorial axis length mostly ≥45 µm: /*Cryptostomata*

1b. Equatorial axis length mostly <45 µm: /*Phanerostomata*

/Phanerostomata:

2a. Exine surface distinctly rugulate, polar axis/pore diameter ratio >3.10:

/P1

2b. Exine surface psilate, apparently faintly reticulate, or otherwise not distinctly rugulate:

3.

3a. Polar axis > 33 µm *B. grandis (/P1)*

3b. Polar axis ≤30 µm, polar axis/pore diameter <3.72:

/P2

Phanerostomata clade P2*:*

Pollen grains strongly biconvex */P2SW*

Pollen grain linear to plano-convex */P2E*

2.1.2. Fossil pollen

Banksia /Cryptostomata* cf. *B. serrata (Proteales: Proteaceae)

(Fig. S6*P*, *Q*)

Description: Monad, anisopolar, outline in equatorial view, crescent shaped, pores 2, 4-9 µm wide with wide collar, exine 1.3-2.7 µm thick with several distinct layers, sculpture punctate to faintly reticulate. Dimensions (unacetolysed): equatorial axis 33-42 µm, polar axis 16-26 µm.

544 *Botanical affinity: Banksia /Cryptostomata sensu* Mast and Givnish 2002. (Figs. S5*G*, and
545 S6*R*, *S*)
546
547 *Discussion*: Acetolysed pollen of extant *B. serrata* is monad, anisopolar, outline in equatorial
548 view crescent-shaped; pores 2, 6-9 µm wide with wide collar, exine 1.5-3 µm thick with
549 several distinct layers, sculpture punctate to faintly reticulate. Dimensions: equatorial axis
550 47-57 µm, polar axis 20-29 µm.
551
552 This thick-walled, crescent-shaped *Banksia* type with several distinct exine layers is
553 consistent with the "*Banksia serrata* type" identified in some southeastern Australian late
554 Quaternary palynological studies (74, 75) and with Paleogene and Neogene *Banksieaeidites*
555 sp. cf. *Banksia serrata* of Macphail (66). However, while they share the general morphology
556 of extant *B. serrata*, the fossil grains are consistently smaller (Figs. S5*A*, *B* and 8*P*-*S*). We
557 attribute this difference to the use of acetolysis during the processing of the modern pollen,
558 and its avoidance during the processing of fossil pollen, because acetolysis is known to
559 increase the size of pollen grains (76). Similar size differences were noted (see below) for
560 fossil *Banksia* pollen we attribute to /*Phanerostomata*. Preliminary examination of pollen of
561 several extant species of /*Cryptostomata* indicated that pollen more or less indistinguishable
562 from *B. serrata* can be found in some distantly related species (Fig. S6*R*, *S*), while that
563 pollen of other /*Cryptostomata* species have pollen which could not be mistaken for that of
564 *B. serrata* (e.g. *B. baueri*, with a thin, psilate exine, and pores lacking a pronounced collar,
565 positioned offset from the narrow ends of the grain). Based on these observations, we
566 tentatively infer that the "*B. serrata* type" represents either a recurrent, homoplastic
567 syndrome, or a generalized plesiomorphic type (77) within /*Cryptostomata*. We thus do not
568 interpret fossil "*B. serrata* type" as representing extant *B. serrata* or its direct ancestor, but
569 simply as a member of *Banksia* /*Cryptostomata*.

570

571 ***Banksia* cf. /*Phanerostomata***

572 ***Banksia* cf. /*Phanerostoma* P2E** (Proteales: Proteaceae)

573 (Fig. S6*I-L*)

574

575 *Description*: Monad, anisopolar, outline in equatorial view rectangular to plano-convex, but
576 weakly ellipsoidal to rectangular when (often) oriented in polar view. Pores 2, 4-12 µm
577 wide, sculpture faintly reticulate. Dimensions (unacetolysed, $n = 29$): equatorial axis 19-36
578 µm, polar axis 13-22 µm.

579

580 *Botanical affinity*: *Banksia* /*Phanerostomata* [*sensu* Mast and Givnish 2002], clade P2E
581 (Figs S5*G*, and S6*M-O*)

582

583 ***Banksia* cf. /*Phanerostomata* P2SW** (Proteales: Proteaceae)

584 (Fig. S6*T*, *U*)

585

586 *Description:* Monad, anisopolar, outline in equatorial view usually strongly biconvex or
587 barrel shaped. Pores 2, 3-7 µm wide, sculpture apparently psilate to faintly reticulate.
588 Dimensions (unacetolysed, $n = 6$): equatorial axis 18-29 µm, polar axis 14-22 µm.

589

590 *Botanical affinity*: *Banksia* /*Phanerostomata* [*sensu* Mast and Givnish (5)], clade P2SW
591 (Figs S5*G*, and S6*V*, *W*)

592

593 *Discussion*: As noted above, equatorial axis length largely distinguishes modern pollen of
594 *Banksia* clade C from clade P. The fossil pollen grains are systematically smaller in size than
595 modern grains because the former were not acetolysed, but the distinction between larger

596 grains, attributable to cf. *B. serrata*, and smaller grains, consistent with /*Phanerostomata*,
597 persists among the fossil grains (Fig. S5*A*, Table S2). We therefore conclude that the small,
598 unacetolysed fossil *Banksia* pollen grains with equatorial axes generally <35 µm long and
599 mostly <30µm long, represent fossils of /*Phanerostomata* (herein abbreviated Pf). For these
600 fossil grains, the ratio of polar axis length to internal pore diameter is significantly different
601 from this ratio in modern pollen of clade P1, but is indistinguishable from modern pollen of
602 clade P2 (Table S2, Fig. S5*C*, *D*). In addition, none of the fossil grains has the conspicuously
603 rugulate exine sculpture (Fig. S6*X*) which characterizes most extant species of clade P1. We
604 therefore interpret these fossil grains as belonging to clade P2. For these grains, the ratio of
605 the radius of curvature to the polar axis (plotted for convenience in Fig. S5*E* as the
606 equivalent ratio, equatorial axis/polar axis vs. equatorial axis/radius of curvature) is
607 significantly different from this ratio in modern pollen of clade P2SW ($p = 0.000$), but it is
608 indistinguishable from modern pollen of clade P2E ($p = 0.409$, Table S2). The fossil pollen
609 attributed to clade P2 thus plots predominantly within the Cartesian space occupied by clade
610 P2E (Fig. S5*E*), and we interpret these fossils as representing the extant clade P2E, currently
611 confined to eastern and northern Australia. However, a small number of grains plot within
612 Cartesian space occupied solely by clade P2SW (Fig.S5*E*, *F*). These fossil grains have a
613 strongly biconvex amb which was not observed in any extant species of clade P2E. The
614 simplest interpretation of this pattern is that the fossil grains which we attribute to clade P2
615 mostly have affinity with eastern and northern Australian clade P2E, but that a small number
616 of grains have affinity to the endemic southwestern Australian clade P2SW.
617
618 **_Geniostoma_ (Gentianales: Loganiaceae)**
619 (Fig. S6*E*-*H*)
620

Description: Monad, isopolar, pores prominent, costate, 3 to 5 in number, 7.2-(8.3)-9.3 µm in diameter, pores not lying in one plane in some 4- and 5-porate grains. Exine psilate or faintly rugulate, 1.3 µm at equator, widening to 1.5-2.2 µm near pores, nexine thickening near endoapertures. Shape: polar view, angulaperturate; equatorial view, oblate to oblate-spheroidal. Dimensions: equatorial axis 29 µm; polar axis 23 µm.

Botanical affinity: *Geniostoma* (Loganiaceae)

Discussion:

This fossil pollen type with 3-5 pores, grains with ≥4 pores typically not lying in one plane, with psilate or faintly rugulate exine, and prominent nexine thickening near endoapertures, corresponds closely to the pollen of *Geniostoma* (Loganiaceae). Pollen of modern species was illustrated previously (78-80). Pollen of some endemic Hawaiian *Labordia* [*viz*. Type 1 of Selling (78)], and *Geniostoma*-type of Punt and Leenhouts (79)) are indistinguishable from that of *Geniostoma*, consistent with Gibbons et al's (81) reduction of *Labordia* to synonymy with *Geniostoma* based on their finding that *Geniostoma* was paraphyletic with respect to *Labordia*. The sister clade to *Geniostoma* is ambiguous. Using chloroplast petD and nuclear ribosomal ETS, Gibbons et al. (81) found that *Geniostoma*+*Labordia* were sister to *Mitrasacme*+(*Phyllangium*+*Schizacme*), though the latter clade included one species of polyphyletic *Mitreola*. Using chloroplast regions petD and rps16, Foster et al. (82) recovered a phylogeny in which *Logania* sect. *Logania* is sister to *Geniostoma*+(*Mitreola*+*Logania* sect. *Stomandra*), and Foster et al. (83) erected *Orianthera* to accommodate *Logania* sect. *Stomandra*. However, the polyporate pollen of *Geniostoma* cannot be mistaken for tricolporate *Logania*, and all other genera within Loganiaceae appear to produce tricolporate or tricolpate pollen (79). Polyporate pollen with pores variably numbering 2-5 occur in Apocynaceae (in Australasia, *viz*. *Parsonsia*) but the exine in *Parsonsia* is very thin, with

protruding pores that have jagged margins (80, 84). We therefore conclude that the fossil represents *Geniostoma*.

Geniostoma species are small trees to small shrubs, sometimes scandent. The genus (including *Labordia*) is distributed from the Mascarene Islands, Malesia, Micronesia, Solomon and New Hebrides Islands, northeastern Australia, Lord Howe Island, northern New Zealand, Polynesia to Hawaii and Marquesas (85) (Fig. S2). In Australia, *Geniostoma rupestre* var *australianum* (F.Muell) B.J. Conn is an understory shrub or small tree in north Queensland rainforest (Australian Tropical Rainforest Plants, available at: http://www.anbg.gov.au/cpbr/cd-keys/rfk/). Two species occur on Lord Howe Island: *Geniostoma huttoni* is a scrambling shrub of dwarf closed forest on ridge tops, while *G. petiolosum* is a small tree to 5 m, occurring in forest at lower altitudes (*Flora of Australia*, Volume 49, 1994). One species, *G. ligustrifolium*, a ruderal, early successional shrub (86), occurs in New Zealand southwards to c. 41.5°S [ref (87)](Fig. S2*K*, *L*).

Doryanthes **(Asparagales: Doryanthaceae)**

(Fig. S6*A*-*C*)

Description: Monad, anisopolar, monosulcate, sulcus extending the full length of the grain, margins ragged. Pollen ellipsoidal to obovate in equatorial view. Exine tectate, reticulate, simplicolumellate, with discrete columellae supporting the muri. Muri arranged in irregular polygonal shapes or rings, approaching a croton pattern on the side opposite the sulcus. Lumina diameter 1.6 µm, becoming smaller, and breaking down into a rugulate pattern, towards the sulcus. Exine thickness 2.2 µm along the longest grain axis, thinning to 1.7 µm along the short grain axis, sexine and nexine of similar thickness. Dimensions: equatorial axis 57 µm; polar axis 40µm.

673

674 *Botanical affinity*: *Doryanthes* (Doryanthaceae)

675

676 *Discussion*: Several features of the fossil – its size, exine thickness, simplicolumellate
677 pattern (Fig. S6*C*), and its polygonal to croton-like lumina decreasing in size and breaking
678 down into a rugulate pattern towards the sulcus (Fig. S6*B*) – correspond closely with the
679 pollen of *Doryanthes*. These features distinguish this type from similarly large, robust
680 (relatively thick exine with nexine and sexine of similar thickness), monosulcate pollen types
681 of the Asparagales and Liliales.

682

683 However, monosulcate, ellipsoidal, reticulate pollen is apparently the plesiomorphic
684 condition within the Asparagales and Liliales, and identification of fossil pollen with these
685 characteristics has typically been at coarse taxonomic level, in both the Quaternary
686 paleoecological and pre-Quaternary palynostratigraphic literatures. For example, for the past
687 half century, monosulcate, reticulate, more or less ellipsoidal grains have routinely been
688 referred to in the Quaternary literature imprecisely as “Liliaceae” (e.g. refs [(88, 89)]), while
689 in the palynostratigraphic literature they are typically assigned to species of *Liliacidites*
690 Couper (e.g. ref [(66)]). Attribution of these pollen type to extant taxa or clades has been
691 inhibited by their lack of conspicuous pollen morphological variability, pervasive
692 homoplasies (90), and, historically, by poor understanding of the evolutionary relationships
693 of monocots (91).

694

695 Guided by current molecular phylogenetic frameworks for monocots, below we note
696 palynological characteristics which distinguish Nullarbor fossil *Doryanthes* from several
697 clades within Asparagales/Liliales, with an emphasis on families currently present in
698 Australasia, based on a combination of published descriptions and our own observations

699 (where relevant, numbers following species names refer to MEL accession numbers).
700 Circumscription of taxa follows the Angiosperm Phylogeny Website wherever possible
701 (available at http://www.mobot.org/MOBOT/Research/APweb/welcome.html).
702
703 Relationships between Doryanthaceae and other Asparagales remain poorly resolved, but
704 until recently Doryanthaceae was hypothesized to be sister to Iridaceae+Ixioliriaceae (92).
705 The large, sulcate, reticulate pollen of some Iridaceae genera is broadly similar to that of the
706 fossil, and several of this family's plesiomorphic clades are endemic to Australia (93).
707 Following the chloroplast phylogeny of Goldblatt et al. (93), the most plesiomorphic clade,
708 monotypic Isophysidoideae, represented by *Isophysis tasmanica* [MEL 1523724] produces
709 pollen smaller than the fossil (equatorial axis 35-40 µm), and its exine is reticulate to
710 retipilate, heterobrochate with lumina up to ~4 µm diameter. In Goldblatt et al's second-
711 branching clade, Patersonioideae, *Patersonia occidentalis* has inaperturate, coarsely
712 reticulate pollen that tends to disintegrate under acetolysis. The pollen of Aristeoideae,
713 confined to Africa and Madagascar, and of Nivenioideae, confined to the Cape region of
714 South Africa, mostly have tectate reticulate exines that are not simplicolumellate under light
715 microscopic LO examination (94-96), and in which the lumina do not generally become
716 smaller as they approach the sulcus (94). The remainder of the family is represented by the
717 species-rich Crocoideae and Iridoideae. The most plesiomorphic Iridoideae clade,
718 Diplarreneae, represented by Australian *Diplarrena*, produces inaperturate pollen (97) or has
719 a poorly defined, smooth area on one face (96). *D. moraea* pollen is ellipsoidal to spheroidal,
720 with exine sculpture obscurely reticulate under bright-field light microscopy, perhaps
721 fossulate judging from scanning electron micrographs (96). Iridoideae pollen are typically
722 monosulcuate, tectate columellate with a reticulate exine (96). Australian Iridoideae genera
723 include *Orthrosanthus (O. polystachyus* MEL 1523154], with a very dense reticulum
724 forming minute (≤1 µm) lumina. The exine of African *Dietes* (e.g. *D. grandiflora*) is

725 simplicolumellate to retipilate, with anastomosing muri which do not break down into a
726 rugulate pattern close to the sulcus. Crocoideae mostly have scabrate, rather than reticulate
727 sculpturing (98). The pollen of *Watsonia* [*W.* ?*borbonica* MEL 2291132] and of *Romulea* [*R.*
728 *rosea*, MEL 693772] is elongated, some grains having apiculate apices. Both genera have a
729 verrucate, rather than reticulate exine sculpture.
730
731 Within Asphodelaceae, pollen of *Xanthorrhoea* (Xanthorrhoeoideae) is smaller (c. 40 x 35
732 µm) than the fossil, with angular, irregular-shaped lumina circumscribed by thick muri that
733 are not simplicolumellate. Hemerocallidoideae are characterized by trichotomosulcate pollen
734 (99). The pollen of *Bulbine* (Asphodeloideae) is microreticulate to fossulate under SEM
735 (100), or finely rugulate under bright field light microscopy.
736
737 In Amaryllidaceae, pollen of *Callostemma* [*C. luteum* MEL 285197] is large (60-70 µm) and
738 reticulate but with very small (<1µm) lumina and muri which are not simplicolumellate;
739 pollen of *Crinum* [*C. flaccidum* MEL 2352573] is large (to 80µm) with sparsely echinate
740 exine sculpture.
741
742 In Boryaceae, pollen of *Borya sphaerocephala* [MEL 227391] is small (c. 30-40µm long),
743 shortly ellipsoid, with a polygonal/vermiform reticulum. In Blandfordiaceae, pollen of
744 *Blandfordia* has a granular exine (101). In Asteliaceae, pollen of *Astelia* is monosulcate and
745 prominently echinate (84). In Hypoxidaceae, *Hypoxis* is finely reticulate, not
746 simplicolumellate, and smaller than the fossil.
747
748 Pollen of Asparagaceae is generally smaller, with thinner exine, than the fossil. Pollen in the
749 Lomandroideae, (e.g. *Arthropodium milleflorum*) is reticulate, with lumina becoming smaller
750 towards the gaping sulcus but not breaking down into a rugulate pattern. Pollen of

Thysanotus tuberosus is typically much smaller than the fossil and has a reticulum with large lumina. Pollen of *Lomandra* and of *Acanthocarpus canaliculatus* [MEL 2211734] is zonosulcate.

Within the Liliales, Campynemataceae comprises two Australasian genera. The sulcate pollen of *Campynema* is small, with foveolate/reticulate exine and multicolumellate muri (102), while *Campynemanthe* is inaperturate (97). *Ripogonum* (Ripogonaceae) is smaller than the fossil, with finer reticulum, and is not simplicolumellate (103). In Colchicaceae, pollen of the Australian taxa *Burchardia* and *Wurmbea* are much smaller than the fossil, with finely reticulate exine sculpture.

Within the Commelinales, pollen in the Haemodoraceae is either bi-, tri- or polyporate (Conostylidoideae), or, under light microscopy, obscurely monosulcate (Haemodoroideae) (104, 105). Pollen of Philydraceae occurs in tetrads (*Philydrum*), or is monosulcate but small (25-40 μm) with exine sculpture that is obscure under light microscopy (106). In the currently unplaced commelinid family Dasypogonaceae (107), the pollen of *Calectasia* has clearly differentiated sexine and nexine similar to the fossil, and has a very fine, simplicolumellate reticulum in which, in contrast to the fossil, the lumina are approximately the same size as the individual columellae, and there is no change in the reticulum as it approaches the sulcus margin. *Baxteria australis* [MEL 2216188] has a retipilate exine in which the apertures are arranged in a pantocolpate or clypeate (108, 109) pattern. *Dasypogon hookeri* [MEL 2025855] is small and microreticulate, with lumina <1μm diameter. In *Kingia*, the sulcus extends around more than half of the grain (108).

Comments:

776 Monotypic, Australian endemic Doryanthaceae comprises two giant-rosette species.
777 *Doryanthes excelsa* occupies near-coastal sclerophyll forests and woodlands on well drained,
778 usually sandstone-derived soils in New South Wales. *D. palmeri* occupies rocky outcrops in
779 of wet sclerophyll forest within a small, near-coastal range straddling the New South
780 Wales/Queensland border (110).

781

SUPPLEMENTARY FIGURE LEGENDS

Figure S1. **Information about locations mentioned in the text. (**A) Australian mean annual precipitation, 1901-2010, derived from Global Precipitation Climatology Centre (GPCC) V6 at 0.5° resolution (111), plotted with Climate Explorer (112) (climexp.knmi.nl/). Green circles, locations of the five caves from which fossil pollen was recovered. (B) Digital Elevation Model (3 second SRTM) of the Nullarbor Plain in southern central Australia with locations of the five caves shown, identified by their respective cave numbers. (C) Climate parameters for the five Nullarbor caves. Climatology derived from ANUCLIM (42).

Figure S2. Distribution of individual taxa/clades mentioned in the text and used for reconstruction of mean annual precipitation, within the survey datasets. (A) Distribution of all Australian surveys; (B-J, M) distribution of individual taxa/clades within the Australian survey dataset; (K) distribution of all New Zealand surveys; (L) distribution of *Geniostoma* within the New Zealand survey dataset. (N) Indo-Pacific presence-only occurrence records, derived from the Global Biodiversity Information Facility (www.gbif.org). (O) Distribution of *Geniostoma* (=*Labordia*) within 'pseudo'-surveys in Hawaii.

Figure S3. **Modeled relationships between mean annual precipitation and probability of occurrence for 13 taxa/clades interpreted as the sources of pollen types observed in the Nullarbor pollen assemblages**. Lines of best fit and standard errors shown. (A-L) GAM probability density for each taxon/clade as a function of mean annual precipitation. Density functions were created from binomial GAMs based on the presence/absence of each taxon within the (A-K) Australian survey dataset, and (L) the New Zealand and Hawaiian survey dataset. (M) Relationship between mean annual precipitation and Chenopodiaceae pollen

808 percent, derived from southern Australian pre-European wetland and modern pollen trap data
809 (43, 44, 113), estimated using a Gaussian GAM.
810
811 **Figure S4. Probability density for each of 13 pollen assemblages as a function of mean**
812 **annual precipitation**. Probability density functions represent joint probabilities derived
813 multiplicatively from the component pollen types contributing to each assemblage (indicated
814 by capital letters referring to panels within Fig. S3).
815
816 **Figure S5. Pollen morphological measurements of clades within modern and fossil**
817 ***Banksia*.** Species examined, for /*Cryptostomata*, include *B. ashbyi*, *B. baxteri, B.*
818 *candolleana*, *B. coccinea*, *B. cuneata*, *B. hookeriana*, *B. serrata*, *B. serratuloides*, *B.*
819 *speciosa.* For /*Phanerostomata* P1*, B. grandis*, *B. grossa*, *B. lanata*, *B. sphaerocarpa*, *B.*
820 *violacea*. For /*Phanerostomata* P2E*, B. aquilonia*, *B. canei*, *B. ericifolia*, *B. integrifollia*, *B.*
821 *marginata*, *B. spinulosa*, *B. dentata.* For /*Phanerostomata* P2SW, *B. brownii*, *B. nutans*, *B.*
822 *occidentalis*, *B. quercifolia*, *B. seminuda*, *B. verticillata.*
823
824 **Figure S6**. **Photomicrographs of selected fossil pollen from Nullarbor speleothems**.
825 Scale bar for (A-D) shown in (A); scale bar for (E-W) shown in (E). (A-C) fossil
826 *Doryanthes*, sample 370-11; (D) modern *Doryanthes excelsa*, acetolysed; (E-H) fossil
827 *Geniostoma*, sample 2200-2; (I-L) fossil *Banksia* interpreted as /*Phanerostomata* P2E
828 (eastern clade), from sample 645-15; (M-O) modern pollen of /*Phanerostomata* eastern
829 clade: (M) *B. integrifolia*; (N) *B. aquilonia*; (O) *B. marginata*; (P-Q) fossil *Banksia*
830 interpreted as /*Cryptostomata*, sample 645-15; (R-S) modern pollen of /*Cryptostomata:* (R)
831 *B. candolleana*, (S) *B. serrata*; (T-U) fossil *Banksia* interpreted as /*Phanerostomata* P2SW
832 (southwestern clade), sample 645-15; (V-W) modern pollen of /*Phanerostomata* P2SW: (V)

833 *B. verticillata*; (W) *B*. *quercifolia*. (X) Modern pollen of *Banksia* /*Phanerostomata* 1, *B.*

834 *grossa*, showing rugulate sculpture (not observed in fossil material).

835

SUPPLEMENTARY TABLES

Table S1. Conservative age estimates of Southern Hemisphere data interpreted by Salzmann et al. (21, 62) **as evidence for Late Pliocene vegetation.** Site numbers correspond to ref [(21)]. We excluded Antarctic sites based on uncertainties about their late Neogene age, following Salzmann et al. (62).

Abbreviations: Aus, Australia; PNG, Papua New Guinea; NZ, New Zealand; SA, South Africa.

Notes:

***** Chronostratigraphy is derived from McMinn (114), who commented, "Foram zone N19 and nannoplankton zone CN10 were not recognized in Hole 765B, indicating that much of the Early Pliocene is either absent or…unsampled"… "The absence of foram Zone N18 indicates that the uppermost late Miocene is either absent…or unsampled". (p. 430).

† Key planktic foraminifera have epoch-scale inter-ocean basin diachronous ranges (see Methods).

‡ The visual match of the Yallalie magnetic polarity record with the geomagnetic polarity timescale (61) is reasonable, but it is unconstrained by radiometric or internal (e.g. sedimentation rate estimates) evidence.

§ Khan commented, "Faunally and lithologically it is not easy to separate Pliocene from Pleistocene sediments in the well section (115)(p 268).

|| Described in 1988 as "Late Pliocene", thus probably mostly, if not entirely now Early Pleistocene (116).

¶ Reanalyses by Rossouw and Scott (117) cast doubt on the reality of the fossil pollen data.

Described by the authors as ">4 to 1 Ma".

★ Described by the authors as "2.6-2.8 Ma".

****** The record includes only a small portion attributed to the uppermost Pliocene, as defined in a 1987 palynostratigraphic scheme. Thus the record is probably entirely Early Pleistocene (116)

861 **Table S1.**
862

Site (site number)	Proxy	Source	Age control	Conservative age estimate	Notes
ODP 765, NW Aust (179)	pollen	(118)	marine biostratigraphic comparison (c. 400 km offshore), magnetostratigraphy	Late Pliocene	*
Tempe Downs Borehole, Aust (180)	pollen	(18)	terrestrial biostratigraphic comparison (informal)	Late Miocene to Early Pleistocene	
Namba Fm, Aust (180)	pollen	(18, 119)	palynostratigraphic comparison (±formal)	Late Miocene to Early Pleistocene	
Wipajiri and Tirari Fms, Aust (180-181)	pollen	(18, 120)	palynostratigraphic comparison (±informal)	Late Miocene to Early Pleistocene	
Northern Eyre Peninsula, Aust (180)	pollen	(18, 121)	palynostratigraphic comparison (±informal)	Late Miocene to Early Pleistocene	
Hapuku-1 well, SE Aust (180)	pollen	(18)	marine biostratigraphic comparison (c. 100 km offshore)	Pliocene	†
ODP 815 and 823, NE Aust (182-183)	pollen	(122)	marine biostratigraphic comparison (c. 250 km offshore)	Late Pliocene	
Butchers Creek, Aust (184)	pollen	(123)	palynostratigraphic comparison (±informal)	Late Miocene to Early Pleistocene	
Yallalie, Aust (185)	pollen	(124, 125)	palynostratigraphic comparison (formal); magnetostratigraphy	Late Pliocene	‡
Lake Tay, Aust (186)	pollen	(18, 126)	palynostratigraphic comparison (formal)	Late Miocene to Early Pleistocene	
Lachlan Fm, Aust (189)	pollen	(18, 127)	palynostratigraphic comparison (formal)	Late Miocene to Early Pleistocene	
Lake George, Aust (188)	pollen	(128)	magnetostratigraphy (discontinuous sections)	Late Miocene to Early Pleistocene	
Linda Valley, Aust (193)	pollen	(129)	palynostratigraphic comparison (formal)	Late Pliocene/Early Pleistocene	
Eastern Highlands, NSW, Aust (189)	pollen	(18, 130-132)	palynostratigraphic comparison (formal)	Late Miocene to Early Pleistocene	
Kowai Fm, NZ (196)	pollen	(133)	palynostratigraphic comparison (±informal)	Pliocene/Early Pleistocene	
Five Fingers Peninsula, NZ (197)	pollen	(134)	marine biostratigraphic comparison and palynostratigraphic comparison (±informal)	Pliocene/Early Pleistocene	
Tadmor Group, NZ (198)	pollen	(135)	palynostratigraphic comparison (±informal)	Late Miocene to Early Pleistocene	
ODP 1123, Chatham Rise (199)	pollen	(136, 137)	(c. 1100 km offshore), magnetostratigraphy (long continuous section)	Late Pliocene	
DSDP 262, Timor (177)	pollen	(138)	marine biostratigraphic comparison (c. 75 km offshore)	Early Pleistocene	
Ivirin No. 1 Well, PNG (178)	pollen	(115, 139, 140)	marine biostratigraphic comparison (informal)	Late Miocene to Early Pleistocene	§
Mahakam Delta, Kalimantan (175)	pollen	(141)	palynostratigraphic comparison (±informal)	Early Pleistocene	‖
Laetoli, Tanzania (124, 126)	Pollen/ vertebrates	(117, 142, 143)	terrestrial biostratigraphic comparison (informal), dated pyroclastics	Late Pliocene: but see note	¶
Malawi Rift (125)	vertebrates	(144)	terrestrial biostratigraphic comparison (informal)	Early Pliocene to Early Pleistocene	#
DSDP 532, SW Africa (127)	pollen	(145)	marine biostratigraphic comparison (c. 200 km offshore); magnetostratigraphy (long continuous section)	Late Pliocene	
ODP 1082, SW Africa (128)	pollen	(146)	"wiggle matching" with benthic $\delta^{18}O$ (c. 160 km offshore)	Late Pliocene	
Langebaanweg, SA (129)	pollen	(147, 148)	terrestrial biostratigraphic comparison (informal)	Miocene to Pliocene	
Makapan Valley, SA (130)	vertebrates	(142)	terrestrial biostratigraphic comparison (informal)	Pliocene, perhaps Late Pliocene	
Sterkfontein, SA (131)	wood	(149)	terrestrial biostratigraphic comparison (informal), magnetostratigraphy (short sections)	Early Pleistocene	★
Lauca Basin, Chile (45)	Sediments	(150)	dated pyroclastics	Late Pliocene	
Southern South America (46-47)	vertebrates	(151)	terrestrial biostratigraphic comparison (far field, informal)	Late Miocene to Early Pleistocene	
Buenos Aires Province, Argentina (48)	vertebrates	(152)	magnetostratigraphy (discontinuous/short section)	Pliocene?	
Foz de Amazonas Basin, Brazil (44)	pollen	(153)	palynostratigraphic comparison (200 km offshore)	Early Pleistocene	**

Table S2. Continuous pollen morphological criteria for separation of clades within *Banksia*, and comparisons between modern and fossil *Banksia* pollen.

Abbreviations: Cf, fossil /*Cryptostomata*; Pf, fossil /*Phanerostomta*; P1, P2, P2SW, P2E, extant /*Phanerostomata* clades (see Fig. S5*G*)

Clade comparison	Criterion	Descriptives	Tests
C vs. P	Length of equatorial axis (µm)	**C**: $n = 41$, $\overline{x} = 59.8$ $\sigma^2 = 10.15$ **P**: $n = 134$, $\overline{x} = 34.1$ $\sigma^2 = 6.57$	Levene test of homogeneity of variances: F = 20.9, p = 0.000 (variances are unequal). Two sample t = 15.3, (df = 51) p = 0.000, mean difference = 25.7µm
P1 vs. P2	Polar axis/pore diameter	**P1**: $n = 30$, $\overline{x} = 3.8$ $\sigma^2 = 0.78$ **P2**: $n = 62$, $\overline{x} = 2.6$ $\sigma^2 = 0.36$	Levene test of homogeneity of variances: F = 21.6, p = 0.000 (variances are unequal). Two sample t = 8.4 (df = 35) p = 0.000, mean difference = 1.26
P2 SW vs. P2 E	Radius of curvature/polar axis	**P2SW**: $n = 49$, $\overline{x} = 1.0$ $\sigma^2 = 0.28$ **P2E**: $n = 48$, $\overline{x} = 2.6$ $\sigma^2 = 2.14$	Levene test of homogeneity of variances: F = 9.25, p = 0.003 (variances are unequal). Two sample t = 5.2 (df = 49) p = 0.000, mean difference = 1.62
Cf (cf. *B. serrata*) vs. Pf	Length of equatorial axis	**Cf**: $n = 14$, $\overline{x} = 36.6$ $\sigma^2 = 3.71$ **Pf**: $n = 35$, $\overline{x} = 24.8$, $\sigma^2 = 3.95$	Levene test of homogeneity of variances: F = 0.14, p = 0.709 (variances are equal). Two sample t = 9.7 (df = 47) p = 0.000, mean difference = 11.9
P1 vs Pf	Polar axis/pore diameter	**P1**: $n = 30$, $\overline{x} = 3.8$ $\sigma^2 = 0.78$ **Pf:** $n = 33$, $\overline{x} = 2.6$ $\sigma^2 = 0.67$	Levene test of homogeneity of variances: F = 1.79, p = 0.186 (variances are equal). Two sample t = 6.9 (df =61) p = 0.000, mean difference = 1.3
P2 vs Pf	Polar axis/pore diameter	**P2**: $n = 48$, $\overline{x} = 2.6$ $\sigma^2 = 0.36$ **Pf:** $n = 33$, $\overline{x} = 2.6$ $\sigma^2 = 0.67$	Levene test of homogeneity of variances: F = 5.96, p = 0.016 (variances are unequal). Two sample t = 0.005 (df =42) p = 0.996 mean difference = 0.0006
P2E vs Pf	Radius of curvature/polar axis	**P2E**: $n = 48$, $\overline{x} = 2.6$ $\sigma^2 = 2.14$ **Pf:** $n = 33$, $\overline{x} = 3.1$ $\sigma^2 = 2.89$	Levene test of homogeneity of variances: F = 4.51, p = 0.037 (variances are unequal). Two sample t = 0.83 (df =55) p = 0.409 mean difference = 0.49
P2SW vs Pf	Radius of curvature/polar axis	**P2SW**: $n = 49$, $\overline{x} = 1.0$ $\sigma^2 = 0.28$ **Pf:** $n = 33$, $\overline{x} = 3.1$ $\sigma^2 = 2.89$	Levene test of homogeneity of variances: F = 34.76, p = 0.000 (variances are unequal). Two sample t = 4.2 (df =32) p = 0.000 mean difference = 2.11

Abbreviations: Cf, fossil /*Cryptostomata*; Pf, fossil /*Phanerostomta*; P1, P2, P2SW, P2E, extant /*Phanerostomata* clades (see Fig. S5*G*)

Table S3. U, Pb concentration and isotope ratio data for Nullarbor speleothems found to contain pollen. Sample codes take the form of 'cave number-sample number'. Isotope ratio uncertainties are quoted at the 2σ level. See Methods section for details of age calculations.

Sample ID	Aliquot #	U ppm	Pb ppm	$^{206}Pb/^{204}Pb$	$^{238}U/^{206}Pb$	% error	$^{207}Pb/^{206}Pb$	% error	Correlation coefficient	Isochron type	MSWD	Corrected Age (Ma)	Uncertainty 95% conf.
2121-1	1	0.497	0.0002	27.274	9832.94	28.76	0.46762	27.10	-0.9999	Model 2	4.1	0.41	0.07
	2	0.487	0.0034	14.996	486.29	1.56	0.80937	0.33	-0.4949				
	3	0.511	0.0022	18.667	785.78	1.82	0.79647	0.28	-0.8455				
	4	0.499	0.0032	20.896	526.83	2.91	0.81326	0.63	-0.4708				
645-15	1	0.596	0.0006	97.041	1574.61	4.95	0.17870	20.23	-0.9993	Model 1	1.1	3.47	0.13
	2	0.608	0.0006	90.056	1560.13	4.12	0.17918	16.76	-0.9993				
	3	0.644	0.0006	93.472	1624.96	5.48	0.14865	28.02	-0.9996				
	4	0.579	0.0007	57.497	1440.01	4.73	0.22722	14.19	-0.9994				
	5	0.361	0.0005	51.243	1329.49	6.17	0.26728	14.80	-0.9997				
370-3	1	0.499	0.0037	24.264	396.26	0.92	0.65844	0.36	-0.9711	Model 2	12	3.62	0.14
	2	0.640	0.0086	21.711	230.21	0.49	0.72893	0.15	-0.8175				
	3	0.435	0.0036	23.605	360.79	1.07	0.67145	0.39	-0.9864				
	4	0.627	0.0021	32.272	728.65	2.18	0.51657	1.66	-0.9983				
	5	0.427	0.0049	21.053	265.99	0.89	0.71513	0.30	-0.8012				
	6	0.681	0.0033	26.796	553.68	1.29	0.59403	0.57	-0.9900				
370-1	1	0.815	0.0047	25.285	487.63	1.05	0.62749	0.47	-0.9900	Model 1	9	3.63	0.17
	2	0.777	0.0087	20.416	273.01	0.59	0.71665	1.00	-0.9900				
	3	0.890	0.0152	23.681	186.21	2.00	0.75883	1.18	-0.0256				
370-5	1	0.923	0.0026	33.492	830.04	3.90	0.46695	3.84	-0.9407	Model 1	0.87	3.76	0.12
	2	0.930	0.0013	27.874	1297.16	4.94	0.25525	12.66	-0.9932				
	3	0.945	0.0027	14.500	834.68	5.15	0.46107	5.00	-0.9963				
	4	0.943	0.0009	34.045	1548.26	7.94	0.14079	43.34	-0.9958				
	5	0.910	0.0013	28.129	1319.67	8.75	0.24901	23.19	-0.9999				
645-13	1	1.378	0.0011	188.181	1455.77	1.55	0.11368	10.77	-0.9962	Model 1	1.8	4.14	0.11
	2	1.413	0.0009	326.580	1561.70	1.26	0.06547	16.03	-0.9905				
	3	1.444	0.0013	149.191	1399.94	1.32	0.14249	7.05	-0.9889				
	4	1.444	0.0011	216.937	1528.48	3.11	0.08050	31.95	-0.9963				
370-11	1	2.232	0.0016	443.252	1474.23	1.15	0.08229	11.50	-0.9722	Model 1	0.65	4.15	0.12
	2	2.213	0.0018	157.545	1401.42	0.79	0.10821	5.62	-0.9632				
	3	2.247	0.0015	58.606	1536.02	1.04	0.06605	13.13	-0.9872				
	4	2.233	0.0017	232.751	1446.45	1.13	0.10250	8.72	-0.9515				
	5	2.575	0.0016	487.537	1563.23	0.93	0.05727	13.78	-0.9934				
	6	2.651	0.0021	154.360	1435.06	1.78	0.09496	15.21	-0.9977				
2200-12-4	1	1.264	0.0040	33.669	732.52	1.49	0.46672	1.42	-0.9994	Model 2	12	4.16	0.12
	2	1.161	0.0039	33.516	699.77	1.49	0.47931	1.34	-0.9990				
	3	1.107	0.0025	35.874	898.33	2.05	0.38734	2.75	-0.9996				
	4	1.185	0.0041	31.877	692.44	2.21	0.48329	1.95	-0.9997				
	5	1.236	0.0078	25.580	441.36	1.65	0.61137	0.81	-0.9977				
	6	1.159	0.0428	20.193	88.57	0.23	0.78183	0.10	-0.6037				

2200-2	1	1.251	0.0037	41.316	779.41	1.65	0.47306	1.73	-0.7433	Model 2	6	4.20	0.14
	2	1.189	0.0012	111.950	1372.26	4.02	0.15846	19.04	-0.9947				
	3	1.180	0.0017	30.526	1183.42	3.17	0.25332	8.20	-0.9992				
	4	1.294	0.0020	58.025	1130.91	2.22	0.28262	4.93	-0.9674				
483-9	1	0.208	0.0012	28.839	447.93	3.10	0.55287	2.00	-0.9966	Model 1	2.3	4.89	0.12
	2	0.184	0.0021	24.352	256.55	1.81	0.66543	0.67	-0.9738				
	3	0.217	0.0004	49.213	990.42	5.83	0.25240	15.15	-0.9990				
	4	0.217	0.0005	46.111	866.50	7.51	0.31584	14.11	-0.9996				
	5	0.207	0.0003	94.751	1233.68	10.90	0.10903	80.00	-0.9960				
370-16	1	0.494	0.0006	129.862	1160.43	3.43	0.14086	18.69	-0.9995	Model 2	25	4.97	0.12
	2	0.446	0.0004	159.337	1248.65	6.13	0.08517	59.29	-0.9996				
	3	0.468	0.0005	211.050	1234.01	5.03	0.09162	44.85	-0.9973				
	4	0.477	0.0012	46.703	792.67	2.66	0.34461	4.35	-0.9950				
	5	0.385	0.0012	42.631	680.70	1.93	0.41639	2.33	-0.9498				
	6	0.404	0.0021	29.680	489.96	1.42	0.53473	1.00	-0.9979				
	7	0.376	0.0016	34.344	567.01	1.50	0.48040	1.33	-0.9973				
370-17	1	1.832	0.0354	22.212	158.78	0.15	0.71576	0.11	-0.8208	Model 2	2.7	5.34	0.12
	2	1.657	0.0317	22.309	159.78	0.14	0.71395	0.10	-0.8377				
	3	1.087	0.0200	22.454	165.88	0.22	0.71054	0.11	-0.8202				
	4	0.423	0.0019	33.262	523.67	1.91	0.48798	1.65	-0.9994				
	5	3.090	0.0509	22.800	183.14	0.18	0.70022	0.11	-0.8373				
370-19	1	2.063	0.0390	22.285	162.23	0.21	0.71538	0.11	-0.7858	Model 1	0.017	5.59	0.15
	2	2.050	0.0309	23.151	198.44	0.20	0.69156	0.11	-0.7885				
	3	1.832	0.0333	22.422	167.97	0.22	0.71167	0.11	-0.5780				
	4	1.591	0.0337	21.866	146.12	0.29	0.72609	0.12	-0.7900				
	5	2.227	0.0363	22.844	185.14	0.19	0.70030	0.11	-0.8151				

SUPPLEMENTARY REFERENCES

1. Carrion JS & Scott L (1999) The challenge of pollen analysis in palaeoenvironmental studies of hominid beds: the record from Sterkfontein caves. *Journal of Human Evolution* 36(4):401-408.
2. Munsterman D & Kerstholt S (1996) Sodium polytungstate, a new non-toxic alternative to bromoform in heavy liquid separation. *Review of Palaeobotany and Palynology* 91:417-422.
3. Maher LJ (1972) Nomograms for computing 0.95 confidence limits of pollen data. *Review of Palaeobotany and Palynology* 13:85-93.
4. Mosimann JE (1965) Statistical methods for the pollen analyst: multinomial and negative multinomial techniques. *Handbook of Paleontological Techniques*, eds Kummel B & Raup D (Freeman, San Francisco, California), pp 636-673.
5. Mast AR & Givnish TJ (2002) Historical biogeography and the origin of stomatal distributions in Banksia and Dryandra (Proteaceae) based on their cpDNA phylogeny. *American Journal of Botany* 89(8):1311-1323.
6. He TH, Lamont BB, & Downes KS (2011) *Banksia* born to burn. *New Phytologist* 191(1):184-196.

7. Cardillo M & Pratt R (2013) Evolution of a hotspot genus: geographic variation in speciation and extinction rates in Banksia (Proteaceae). *BMC Evolutionary Biology* 13:155.
8. Punt W, Hoen PP, Blackmore S, Nilsson S, & Le Thomas A (2007) Glossary of pollen and spore terminology. *Review of Palaeobotany and Palynology* 143:1-81.
9. Coles GM & Gilbertson DD (1994) The airfall-pollen budget of archaeologically important caves: Creswell Crags, England. *Journal of Archaeological Science* 21:735-755.
10. Burney DA & Burney LP (1993) Modern Pollen Deposition in Cave Sites - Experimental Results from New-York-State. *New Phytologist* 124(3):523-535.
11. McGarry SF & Caseldine C (2004) Speleothem palynology: an undervalued tool in Quaternary studies. *Quaternary Science Reviews* 23(23-24):2389-2404.
12. Bastin B (1978) L'analyse pollinique des stalagmites: Une nouvelle possibilité d'approche des fluctuations climatiques du Quaternaire. *Annales de la Société Géologique de Belgique* 101:13-19.
13. Navarro C, Carrion JS, Munuera M, & Prieto AR (2001) Cave surface pollen and the palynological potential of karstic cave sediments in palaeoecology. *Review of Palaeobotany and Palynology* 117(4):245-265.
14. Hunt CO & Rushworth G (2005) Pollen taphonomy and airfall sedimentation in a tropical cave: the west mouth of the great cave of Niah in Sarawak, Malaysian Borneo. *Journal of Archaeological Science* 32(3):465-473.
15. Webb JA & James JM (2006) Karst evolution of the Nullarbor Plain, Australia. *Geological Society of America Special Paper* 404:65-78.
16. Newstrom L & Robertson A (2005) Progress in understanding pollination systems in New Zealand. *New Zealand Journal of Botany* 43:1-59.
17. Pagani M, Arthur MA, & Freeman KH (1999) Miocene evolution of atmospheric carbon dioxide. *Paleoceanography* 14:273-292.
18. Macphail MK (1997) Late Neogene climates in Australia: fossil pollen- and spore-based estimates in retrospect and prospect. *Australian Journal of Botany* 45:425-464.
19. Murton JB*, et al.* (2001) A late Middle Pleistocene temperate–periglacial–temperate sequence (Oxygen Isotope Stages 7–5e) near Marsworth, Buckinghamshire, UK. *Quaternary Science Reviews* 20(18):1787-1825.
20. Traverse A (2007) *Paleopalynology* (Springer, Dordrecht, Netherlands) 2nd Ed.
21. Salzmann U, Haywood AM, Lunt DJ, Valdes PJ, & Hill DJ (2008) A new global biome reconstruction and data-model comparison for the Middle Pliocene. *Global Ecology and Biogeography* 17(3):432-447.
22. McGlone MS (2001) A late Quaternary pollen record from marine core P69, southeastern North Island, New Zealand. *New Zealand Journal of Geology & Geophysics* 44:69-77.
23. Beadle N (1981) *The Vegetation of Australia* (Cambridge University Press, New York).
24. Hills RR, Sandiford M, Reynolds SD, & Quigley MC (2008) Present-day stresses, seismicity and Neogene-to-Recent tectonics of Australia's 'passive' margins: intraplate deformation controlled by plate boundary forces. *Geological Society of London, Special Publications* 306:71-90.
25. Sinka KJ & Atkinson TC (1999) A mutual climatic range mthod for reconstructing palaeoclimate from plant remains. *Journal of the Geological Society* 156:381-396.
26. Mosbrugger V & Utescher T (1997) The coexistence approach- a method for quantitative reconstructions of Tertiary terrestrial palaeoclimate data using plant fossils. *Palaeogeography, Palaeoclimatology, Palaeoecology* 134:61-86.

27. Sniderman JMK, Porch N, & Kershaw AP (2009) Quantitative reconstruction of Early Pleistocene climate in southeastern Australia and implications for atmospheric circulation. *Quaternary Science Reviews* 28:3185-3196.
28. Porch N (2010) Climate space, bioclimatic envelopes and coexistence methods for the reconstruction of past climates: a method using Australian beetles and significance for Quaternary reconstruction. *Quaternary Science Reviews* 29(5-6):633-647.
29. DPaW (2007-) *NatureMap: Mapping Western Australia's Biodiversity* (Department of Parks and Wildlife).
30. Elith J & Leathwick JR (2009) Species distribution models: ecological explanation and prediction across space and time. *Annual Review of Ecology, Evolution, and Systematics* 40(1):677-697.
31. Franklin J (2010) *Mapping Species Distributions: Spatial Inference and Prediction* (Cambridge University Press, Cambridge) p 336.
32. Ward GT, Hastie T, Barry S, Elith J, & Leathwick J (2009) Presence-only data and the EM algorithm. *Biometrics* 65:554-563.
33. Elith J*, et al.* (2006) Novel methods improve prediction of species' distributions from occurrence data. *Ecography* 29(2):129-151.
34. Phillips S & Elith J (2013) On estimating probability of presence from use–availability or presence–background data. *Ecology* 94:1409-1419.
35. Fithian W, Elith J, Hastie T, & Keith DA (2014) Bias correction in species distribution models: pooling survey and collection data for multiple species. *Methods in Ecology and Evolution* 6:424-438.
36. Gu WD & Swihart RK (2004) Absent or undetected? Effects of non-detection of species occurrence on wildlife–habitat models. *Biological Conservation* 116:195-203.
37. Chen L-Y*, et al.* (2014) Historical biogeography of Haloragaceae: An out-of-Australia hypothesis with multiple intercontinental dispersals. *Molecular Phylogenetics and Evolution* 78(0):87-95.
38. Price J*, et al.* (2012) *Mapping Plant Species Ranges in the Hawaiian Islands—Developing a Methodology and Associated GIS Layers* p 34.
39. Stevens PF (2001-) *Angiosperm Phylogeny Website. Version 12, July 2012 [and more or less continuously updated since]*.
40. Wood S (2012) *mgcv : Mixed GAM Computation Vehicle with GCV/AIC/REML smoothness estimation*.
41. Team RDC (2003) *R: A language and environment for statistical computing* (Foundation for Statistical Computing, Vienna, Austria).
42. Xu T & Hutchinson M (2011) *ANUCLIM Version 6.1* (ANU Fenner School of Environment and Society, Canberra).
43. D'Costa D & Kershaw AP (1997) An expanded Recent pollen database from south-eastern Australia and its potential for refinement of palaeoclimatic estimates. *Australian Journal of Botany* 45:583-605.
44. Newsome JC (1999) Pollen-vegetation relationships in semi-arid southwestern Australia. *Review of Palaeobotany and Palynology* 106(1-2):103-119.
45. Martin HA (1973) Palynology and historical ecology of some cave excavations in the Australian Nullarbor. *Australian Journal of Botany* 21:283-316.
46. Woodhead J*, et al.* (2006) U–Pb geochronology of speleothems by MC-ICPMS. *Quaternary Geochronology* 1(3):208-221.
47. Woodhead J*, et al.* (2010) Speleothem climate records from deep time? Exploring the potential with an example from the Permian. *Geology* 38:455-458.

997 48. Paton C, Hellstrom J, Paul B, Woodhead J, & Hergt J (2011) Iolite: Freeware for the
998 visualisation and processing of mass spectrometric data. *Journal of Analytical Atomic*
999 *Spectrometry*:2508-2518.
1000 49. Schmitz MD & Schoene B (2007) Derivation of isotope ratios, errors, and error
1001 correlations for U-Pb geochronology using 205Pb-235U-(233U)-spiked isotope
1002 dilution thermal ionization mass spectrometric data. *Geochemistry, Geophysics,*
1003 *Geosystems* 8(8):Q08006.
1004 50. Ludwig KR (2001) Isoplot/Ex, rev. 2.49. A Geochronological Toolkit for Microsoft
1005 Excel. *Berkeley Geochronology Center Special Publication 1a*.
1006 51. Powell R, Hergt J, & Woodhead J (2002) Improving isochron calculations with
1007 robust statistics and the bootstrap. *Chemical Geology* 185:191-204.
1008 52. Jaffey AH, Flynn KF, Glendenin LE, Bentley WC, & Essling AM (1971) Precision
1009 measurement of half-lives and specific activities of 235U and 238U. *Physical Review*
1010 C4:1889-1906.
1011 53. Cheng H*, et al.* (2013) Improvements in 230Th dating, 230Th and 234U half-life
1012 values, and U–Th isotopic measurements by multi-collector inductively coupled
1013 plasma mass spectrometry. *Earth and Planetary Science Letters* 371–372:82-91.
1014 54. Prideaux GJ*, et al.* (2007) An arid-adapted middle Pleistocene vertebrate fauna from
1015 south-central Australia. *Nature* 445(7126):422-425.
1016 55. Garreta V, Guiot J, Mortier F, Chadoeuf J, & Hély C (2012) Pollen-based climate
1017 reconstruction: calibration of the vegetation–pollen processes. *Ecological Modelling*
1018 235-236:81-94.
1019 56. Martin TG*, et al.* (2005) Zero tolerance ecology: improving ecological inference by
1020 modelling the source of zero observations. *Ecology Letters* 8(11):1235-1246.
1021 57. Chen J & Gupta AK (2000) *Parametric Statistical Change Point Analysis*
1022 (Birkhauser, New York).
1023 58. Killick R, Eckley I, Haynes K, & Fearnhead P (2014) *An R package for changepoint*
1024 *analysis*.
1025 59. Killick R, Fearnhead P, & Eckley IA (2012) Optimal detection of changepoints with
1026 a linear computational cost. *Journal of the American Statistical Association*
1027 107:1590-1598.
1028 60. Zachos JC, Dickens GR, & Zeebe RE (2008) An early Cenozoic perspective on
1029 greenhouse warming and carbon-cycle dynamics. *Nature* 451(7176):279-283.
1030 61. Ogg JG (2012) Chapter 5 - Geomagnetic Polarity Time Scale. *The Geologic Time*
1031 *Scale*, eds Gradstein FM, Ogg JG, Schmitz MD, & Ogg GM (Elsevier, Boston), pp
1032 85-113.
1033 62. Salzmann U*, et al.* (2013) Challenges in quantifying Pliocene terrestrial warming
1034 revealed by data-model discord. *Nature Climate Change* 3(11):969-974.
1035 63. Stover LE & Partridge AD (1973) Tertiary and Late Cretaceous spores and pollen
1036 from the Gippsland Basin, south-eastern Australia. *Proceedings of the Royal Society*
1037 *of Victoria* 85:237-286.
1038 64. Partridge AD (2006) Late Cretaceous–Cenozoic palynology zonations Gippsland
1039 Basin. *Australian Mesozoic and Cenozoic Palynology Zonations – Updated to the*
1040 *2004 Geologic Time Scale*, ed Monteil E (Geoscience Australia Record 2006/23).
1041 65. Macphail MK & Truswell EM (1993) Palynostratigraphy of the Bookpurnong Beds
1042 and related late Miocene-early Pliocene facies in the central West Murray Basin; Part
1043 2, Spores and pollens. *AGSO Journal of Australian Geology and Geophysics*
1044 14(4):383-409.
1045 66. Macphail MK (1999) Palynostratigraphy of the Murray Basin, inland southeastern
1046 Australia. *Palynology* 23:197-240.
1047 67. McMinn A (1992) Pliocene through Holocene dinoflagellate cyst biostratigraphy of
1048 the Gippsland Basin, Australia. *Neogene and Quaternary Dinoflagellate Cysts and*

Acritarchs, eds Head MJ & Wrenn JH (American Associatioin of Stratigraphic Palynologists Foundation, Dallas), pp 147-161.
68. Anthonissen DE & Ogg JG (2012) Appendix 3 - Cenozoic and Cretaceous Biochronology of Planktonic Foraminifera and Calcareous Nannofossils. *The Geologic Time Scale*, eds Gradstein FM, Schmitz JGOD, & Ogg GM (Elsevier, Boston), pp 1083-1127.
69. Wade BS, Pearson PN, Berggren WA, & Pälike H (2011) Review and revision of Cenozoic tropical planktonic foraminiferal biostratigraphy and calibration to the geomagnetic polarity and astronomical time scale. *Earth-Science Reviews* 104(1–3):111-142.
70. Gallagher SJ*, et al.* (2003) The Pliocene climatic and environmental evolution of southeastern Australia: evidence from the marine and terrestrial realm. *Palaeogeography Palaeoclimatology Palaeoecology* 193(3-4):349-382.
71. Sniderman JMK (2011) Early Pleistocene vegetation change in upland south-eastern Australia. *Journal of Biogeography* 38:1456-1470.
72. Cookson IC (1950) Fossil pollen grains of Proteaceous type from Tertiary deposits in Australia. *Australian Journal of Science* 3:166-177.
73. Baum DA, Alverson WS, & Nyffeler R (1998) A durian by any other name: taxonomy and nomenclature of the core Malvales. *Harvard Papers in Botany* 3:315-330.
74. Macphail M (1973) Pollen analysis of a buried organic deposit on the backshore at Fingal Bay, Port Stephens, New South Wales. *Proceedings of the Linnean Society of New South Wales* 98:222-233.
75. Hooley AD, Southern W, & Kershaw AP (1980) Holocene vegetation and environments of Sperm Whale Head, Victoria, Australia. *Journal of Biogeography* 7(4):349-362.
76. Reitsma T (1969) Size modification of recent pollen grains under different treatments. *Review of Palaeobotany and Palynology* 9:175-202.
77. Sauquet H*, et al.* (2012) Testing the Impact of Calibration on Molecular Divergence Times Using a Fossil-Rich Group: The Case of Nothofagus (Fagales). *Systematic Biology* 61(2):289-313.
78. Selling OH (1947) *Studies in Hawaiian Pollen Statistics. Part II. The Pollens of the Hawaiian Phanerogams* (Bishop Museum, Honolulu, Hawaii).
79. Punt W & Leenhouts PW (1967) Pollen morphology and taxonomy in the Loganiaceae. *Grana Palynologica* 7:469-516.
80. Moar NT (1993) *Pollen Grains of New Zealand Dicotyledonous Plants* (Maanaki Whenua Press, Lincoln) p 200.
81. Gibbons KL, Henwood MJ, & Conn BJ (2012) Phylogenetic relationships in Loganieae (Loganiaceae) inferred from nuclear ribosomal and chloroplast DNA sequence data. *Australian Systematic Botany* 25:331-340.
82. Foster CSP, Ho SYW, Conn BJ, & Henwood MJ (2014) Molecular systematics and biogeography of *Logania* R.Br. (Loganiaceae). *Molecular Phylogenetics and Evolution* 78(0):324-333.
83. Foster C, Conn BJ, Henwood MJ, & Ho S (2014) Molecular data support *Orianthera*: a new genus of Australian Loganiaceae. *Telopea* 16:149-158.
84. Moar NT, Wilmshurst JM, & McGlone MS (2011) Standardizing names applied to pollen and spores in New Zealand Quaternary palynology. *New Zealand Journal of Botany* 49:201-229.
85. Conn BJ (1980) A taxonomic revision of *Geniostoma* subg. *Geniostoma* (Loganiaceae). *Blumea* 26:245-364.

86. Moles AT & Drake DR (1999) Potential contributions of the seed rain and seed bank to regeneration of native forest under plantation pine in New Zealand. *New Zealand Journal of Botany* 37:83-93.
87. Allan HH (1982) *Flora of New Zealand* (Government Printer, Wellington) p 1085.
88. Heusser CJ (1964) Palynology of four bog sections from the western Olympic Peninsula, Washington. *Ecology* 45:23-40.
89. Moravek S, Luly J, Grindrod J, & Fairfax R (2013) The origin of grassy balds in the Bunya Mountains, southeastern Queensland, Australia. *The Holocene* 23(2):305-315.
90. Furness CA & Rudall PJ (2001) Pollen and anther characters in monocot systematics. *Grana* 40:17-25.
91. Chase MW*, et al.* (2000) Higher-level systematics of the monocotyldeons: an assessment of current knowledge and a new classification. *Monocots: Systematics and Evolution*, eds Wilson KL & Morrison DA (CSIRO, Melbourne), pp 3-16.
92. Chase MW*, et al.* (2006) Multigene analysis of monocot relationships: a summary. *Aliso* 22:63-75.
93. Goldblatt P*, et al.* (2008) Iridaceae 'out of Australasia'? Phylogeny, biogeography, and divergence time based on plastid DNA sequences. *Systematic Botany* 33(3):495-508.
94. Schulze W (1971) Beiträge zur Pollenmorphologie der Iridaceae und ihre Bedeutung für die Taxonomie. *Feddes Repertorium* 82:101-124.
95. Goldblatt P & Manning JC (1989) Pollen Morphology of the Shrubby Iridaceae *Nivenia*, *Klattia*, and *Witsenia*. *Annals of the Missouri Botanical Garden* 76:1103-1108.
96. Goldblatt P & Le Thomas A (1992) Pollen apertures, exine sculpturing and phylogeny in Iridaceae subfamily Iridoideae. *Review of Palaeobotany and Palynology* 75:301-315.
97. Furness CA & Rudall PJ (1999) Inaperturate pollen in monocotyledons. *International Journal of Plant Science* 160:395-414.
98. Goldblatt P, Manning JC, & Bari A (1991) Sulcus and operculum structure in the pollen grains of Iridaceae subfamily Ixoideae. *Annals of the Missouri Botanical Garden* 78:950-961.
99. Furness CA, Conran JG, Gregory T, & Rudall PJ (2014) The trichotomosulcate asparagoids: pollen morphology of Hemerocallidaceae in relation to systematics and pollination biology. *Australian Systematic Botany* 26:393-407.
100. Kosenko V (1999) Pollen morphology in the family Asphodelaceae (Asphodeleae, Kniphofieae). *Grana* 38:218-227.
101. Clifford HT & Conran JG (1998) Blandfordiaceae. *Flowering Plants – Monocotyledons*, ed Kubitzki K (Springer-Verlag, Heidelberg), pp 148-150.
102. Erdtman G (1971) *Pollen Morphology and Plant Taxonomy – Angiosperms* (Hafner, New York) p 553.
103. Chen SC, Zhang XP, Ni SF, Fu CX, & Cameron KM (2006) The systematic value of pollen morphology in Smilacaceae. *Plant Systematics and Evolution* 259:19-37.
104. Simpson MG (1983) Pollen ultrastructure of the Haemodoraceae and its taxonomic significance. *Grana* 22:79-103.
105. Pierce NB & Simpson MG (2009) Polyaperturate pollen types and ratios of heteromorphism in the monocot genus *Conostylis* (Haemodoraceae). *Australian Systematic Botany* 22(1):16-30.
106. Simpson MG (1985) Pollen ultrastructure of the Philydraceae. *Grana* 24:23-31.
107. Barrett CF, Davis JI, Leebens-Mack J, Conran JG, & Stevenson DW (2013) Plastid genomes and deep relationships among the commelinid monocot angiosperms. *Cladistics* 29(1):65-87.

108. Chanda S & Ghosh K (1976) Pollen morphology and its evolutionary significance in Xanthorrhoeaceae. *The Evolutionary Significance of the Exine*, eds Ferguson IK & Muller J (Academic Press, London), pp 527-559.
109. Halbritter H & Hesse M (1995) The convergent evolution of exine shields in angiosperm pollen. *Grana* 34:108-119.
110. Harden G (1993) *Flora of New South Wales* (NSW University Press, Kensingston, NSW) p 775.
111. Schneider U*, et al.* (2011) GPCC Full Data Reanalysis Version 6.0 at 0.5°: Monthly Land-Surface Precipitation from Rain-Gauges built on GTS-based and Historic Data).
112. van Oldenborgh GJ*, et al.* (2009) Western Europe is warming much faster than expected. *Climate of the Past* 5:1-12.
113. Martin HA (1973) The palynology of some Tertiary and Pleistocene deposits, Lachlan River Valley, New South Wales. *Australian Journal of Botany* Supplementary series 6:1-57.
114. McMinn A (1992) Neogene dinoflagellate distribution in the eastern Indian Ocean from Leg 123, Site 765. *Proceedings of Ocean Drilling Program Scientific Results* 123:429-441.
115. Khan AA (1974) Palynology of Neogene sediments from Papua (New Guinea) stratigraphic boundaries. *Pollen et Spores* 16:265-284.
116. Gibbard PL, Head MJ, & Walker MJC (2010) Formal ratification of the Quaternary System/Period and the Pleistocene Series/Epoch with a base at 2.58 Ma. *Journal of Quaternary Science* 25(2):96-102.
117. Rossouw L & Scott L (2011) Phytoliths and pollen, the microscopic plant remains in Pliocene volcanic sediments around Laetoli, Tanzania. *Paleontology and Geology of Laetoli: Human Evolution in Context. Volume 1: Geology, Geochronology, Paleoecology and Paleoenvironment.*, ed Harrison T (Springer, Dordrecht), Vol 1, pp 201-215.
118. Martin HA & McMinn A (1994) Late Cainozoic vegetation history of north-western Australia, from the palynology of a deep sea core (ODP Site 765). *Australian Journal of Botany* 42:95-102.
119. Martin HA (1990) The palynology of the Namba Formation in Wooltana-1 bore, Callabona Basin (Lake Frome), South Australia and its relevance to Miocene grasslands in central Australia. *Alcheringa* 14:247-255.
120. Callen RA, Alley NF, & Greenwood DR (1995) Lake Eyre Basin. *South Australian Geological Survey Bulletin* 54:188-194.
121. Truswell EM & Harris WK (1982) The Cainozoic palaeobotanical record in arid Australia: fossil evidence for the origins of an arid adapted flora. *Evoluton of the Flora and Fauna of Arid Australia*, eds Barker WR & Greenslade PJM (Peacock, Adelaide), pp 67-76.
122. Martin HA & McMinn A (1993) Palynology of sites 815 and 823: the Neogene vegetation history of coastal northeastern Australia. *Proceedings of Ocean Drilling Program Scientific Results* 133:115-123.
123. Kershaw AP & Sluiter IRK (1982) Late Cenozoic pollen spectra from the Atherton Tableland, north-eastern Australia. *Australian Journal of Botany* 30:279-295.
124. Dodson JR & Macphail MK (2004) Palynological evidence for aridity events and vegetation change during the Middle Pliocene, a warm period in southwestern Australia. *Global and Planetary Change* 41:285-307.
125. Dodson JR & Ramrath A (2001) An Upper Pliocene lacustrine environmental record from south-Western Australia- preliminary results. *Palaeogeography, Palaeoclimatology, Palaeoecology* 167:309-320.

126. Bint AN (1981) An early Pliocene pollen assemblage from Lake Tay, southwestern Australia, and its phytogeographic implications. *Australian Journal of Botany* 29:277-291.
127. Martin HA (1991) Tertiary stratigraphic palynology and palaeoclimate of the inland river systems in New South Wales. *The Cainozoic of Australia: a Re-appraisal of the Evidence,* Special Publication of the Geological Society of Australia, eds Williams MAJ, De Deckker P, & Kershaw AP), Vol 18, pp 181-194.
128. Kershaw AP, Martin HA, & McEwan Mason JRC (1994) The Neogene: a period of transition. *History of the Australian Vegetation: Cretaceous to Recent*, ed Hill RS (Cambridge University Press, Cambridge), pp 299-327.
129. Macphail MK, Colhoun EA, & Fitzsimons SJ (1995) Key periods in the evolution of the Cenozoic vegetation and flora in western Tasmania: the Late Pliocene. *Australian Journal of Botany* 43:505-526.
130. Martin HA (1979) Stratigraphic palynology of the Mooki Valley, New South Wales. *Journal and Proceedings of the Royal Society of New South Wales* 112:71-78.
131. Martin HA (1980) Stratigraphic palynology from shallow bores in the Namoi River and Gwydir River valleys, North-central New South Wales. *Journal and Proceedings of the Royal Society of New South Wales* 113, Parts 3 and 4(317-318):81-87.
132. Martin HA (1981) Stratigraphic palynology of the Castlereagh River valley, New South Wales. *Journal and Proceedings of the Royal Society of New South Wales* 114(321-322):77-84.
133. Mildenhall DC (2001) Pollen analysis of Pliocene-Pleistocene Kowai Formation (Kurow Group), Mackenzie Basin, South Canterbury, New Zealand. *New Zealand Journal of Geology and Geophysics* 44(1):97-104.
134. Turnbull IM, Lindqvist JK, Mildenhall DC, Hornibrook NdB, & Beu AG (1985) Stratigraphy and paleontology of Pliocene-Pleistocene sediments on Five Fingers Penninsula, Dusky Sound, Fiordland. *New Zealand Journal of Geology & Geophysics* 28:217-231.
135. Mildenhall D & Suggate RP (1981) Palynology and age of the Tadmor Group (Late Miocene-Pliocene) and Porika Formation (early Pleistocene), South Island, New Zealand. *New Zealand Journal of Geology & Geophysics* 24:515-528.
136. Mildenhall DC (2003) Deep-sea record of Pliocene and Pleistocene terrestrial palynomorphs from offshore eastern New Zealand (ODP Site 1123, Leg 181). *New Zealand Journal of Geology and Geophysics* 46(3):343-361.
137. Mildenhall DC, Hollis CJ, & Naish TR (2004) Orbitally-influenced vegetation record of the Mid-Pleistocene climate transition, offshore eastern New Zealand (ODP Leg 181, Site 1123). *Marine Geology* 205(1-4):87-111.
138. Zaklinskaya ED (1978) Palynological information from Late Pliocene-Pleistocene deposits recovered by deep-sea drilling in the region of the island of Timor. *Review of Palaeobotany and Palynology* 26:227-241.
139. Khan AA (1976) Palynology of Tertiary sediments from Papua New Guinea. II. Gymnosperm pollen from upper Tertiary sediments. *Australian Journal of Botany* 24:783-791.
140. Khan AA (1976) Palynology of Tertiary sediments from Papua New Guinea. I. New form genera and species from upper Tertiary sediments. *Australian Journal of Botany* 24:753-781.
141. Caratini C & Tissot C (1988) Paleogeographical evolution of thge Mahakam Delta in Kalimantan, Indonesia during the Quaternary and Late Pliocene. *Review of Palaeobotany and Palynology* 55:217-228.
142. Reed KE (1997) Early hominid evolution and ecological change through the African Plio-Pleistocene. *Journal of Human Evolution* 32(2–3):289-322.

143. Bonnefille R & Riollet G (1987) Palynological spectra from the Upper Laetolil Beds. *Laetoli: A Pliocene Site in Northern Tanzania*, eds Leakey MD & Harris JH (Clarendon Press, Oxford), pp 52-61.
144. Schrenk F, Bromage TG, Gorthner A, & Sandrock O (1995) Paleoecology of the Malawi Rift: Vertebrate and invertebrate faunal contexts of the Chiwondo Beds, northern Malawi. *Journal of Human Evolution* 28:59-70.
145. Dowsett H & Willard D (1996) Southeast Atlantic marine and terrestrial response to middle Pliocene climate change. *Marine Micropaleontology* 27:181-193.
146. Dupont LM, Donner B, Vidal L, Pérez EM, & Wefer G (2005) Linking desert evolution and coastal upwelling: Pliocene climate change in Namibia. *Geology* 33:461-464.
147. Tankard AJ & Roger J (1978) Late Cenozoic palaeoenvironments of the west coast of Southern Africa. *Journal of Biogeography* 5:319-337.
148. Roberts DL*, et al.* (2011) Regional and global context of the Late Cenozoic Langebaanweg (LBW) palaeontological site: West Coast of South Africa. *Earth-Science Reviews* 106(3–4):191-214.
149. Bamford M (1999) Pliocene fossil woods from an early hominid cave deposit, Sterkfontein, South Africa. *South African Journal of Science* 95:231-237.
150. Gaupp R, Kött A, & Wörner G (1999) Palaeoclimatic implications of Mio–Pliocene sedimentation in the high-altitude intra-arc Lauca Basin of northern Chile. *Palaeogeography, Palaeoclimatology, Palaeoecology* 151(1–3):79-100.
151. Pascual R & Ortiz Jaureguizar E (1990) Evolving climates and mammal faunas in Cenozoic South America. *Journal of Human Evolution* 19:23-60.
152. Zarate MA & Fasano JL (1989) The Plio-Pleistocene record of the central eastern Pampas, Buenos Aires province, Argentina: The Chapadmalal case study. *Palaeogeography, Palaeoclimatology, Palaeoecology* 72(0):27-52.
153. Carvalho MA (2003) Paleoecological and paleoclimatic studies based on palynology of Pliocene and Pleosticene sediments from the Foz do Amazonas, Brazil. *Neues Jahrbuch für Geologie und Paläeontologie* 229:1-18.

Figure S1

A

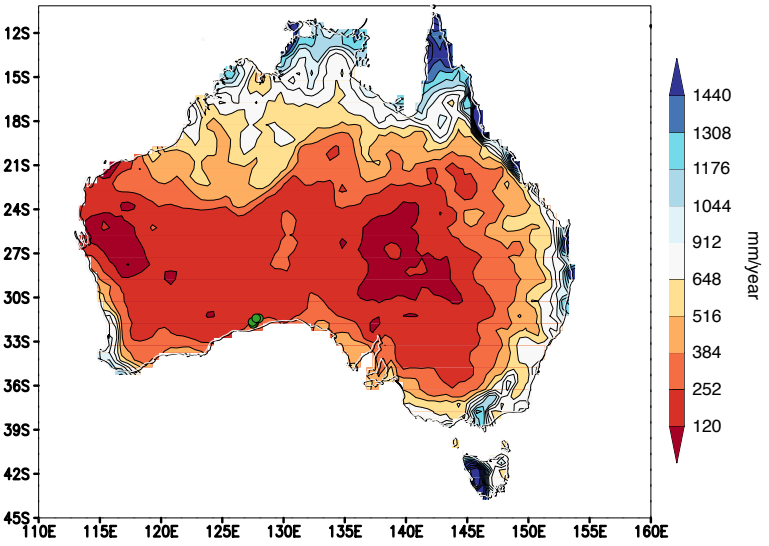

B

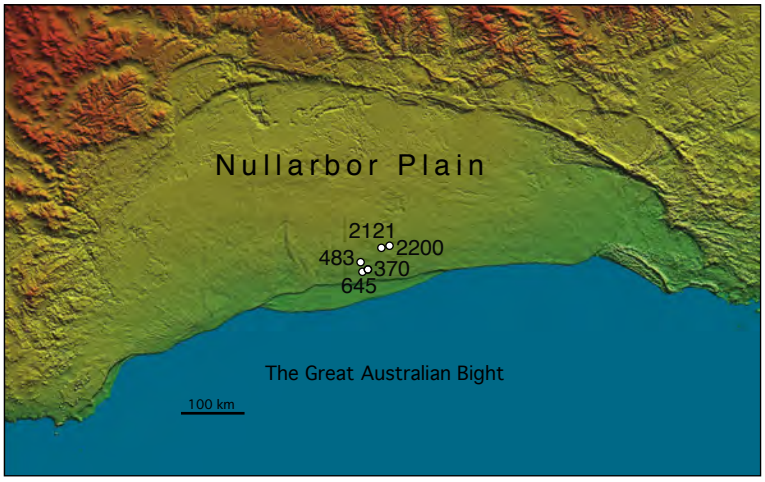

C

Cave number (name)	Location	MAP (mm)	MAT (°C)
370 (Matilda)	31.8°S, 127.8°E	262	17.6
483 (Hurricane Hole)	31.7°S, 127.7°E	251	17.6
645 (Windy Hollow)	31.8°S, 127.7°E	265	17.5
2200 (Leaena's Breath)	31.4°S, 128.1°E	239	17.8
2121 (Last Tree Cave)	31.4°S, 127.9°E	233	17.8

Figure S2

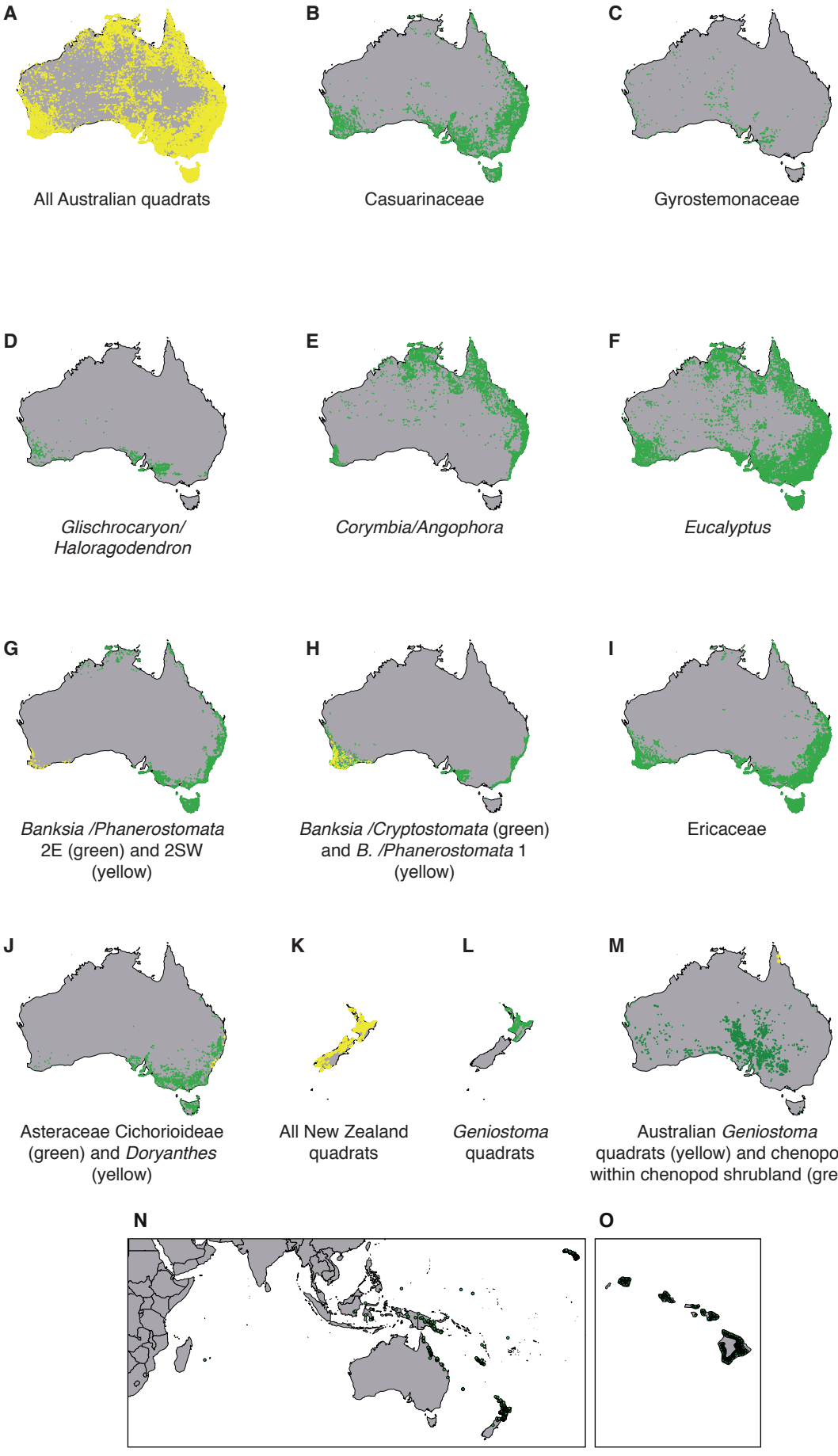
A
All Australian quadrats
B
Casuarinaceae
C
Gyrostemonaceae
D
Glischrocaryon/ Haloragodendron
E
Corymbia/Angophora
F
Eucalyptus
G
Banksia /Phanerostomata 2E (green) and 2SW (yellow)
H
Banksia /Cryptostomata (green) and *B. /Phanerostomata* 1 (yellow)
I
Ericaceae
J
Asteraceae Cichorioideae (green) and *Doryanthes* (yellow)
K
All New Zealand quadrats
L
Geniostoma quadrats
M
Australian *Geniostoma* quadrats (yellow) and chenopods within chenopod shrubland (green)
N
O

Figure S3

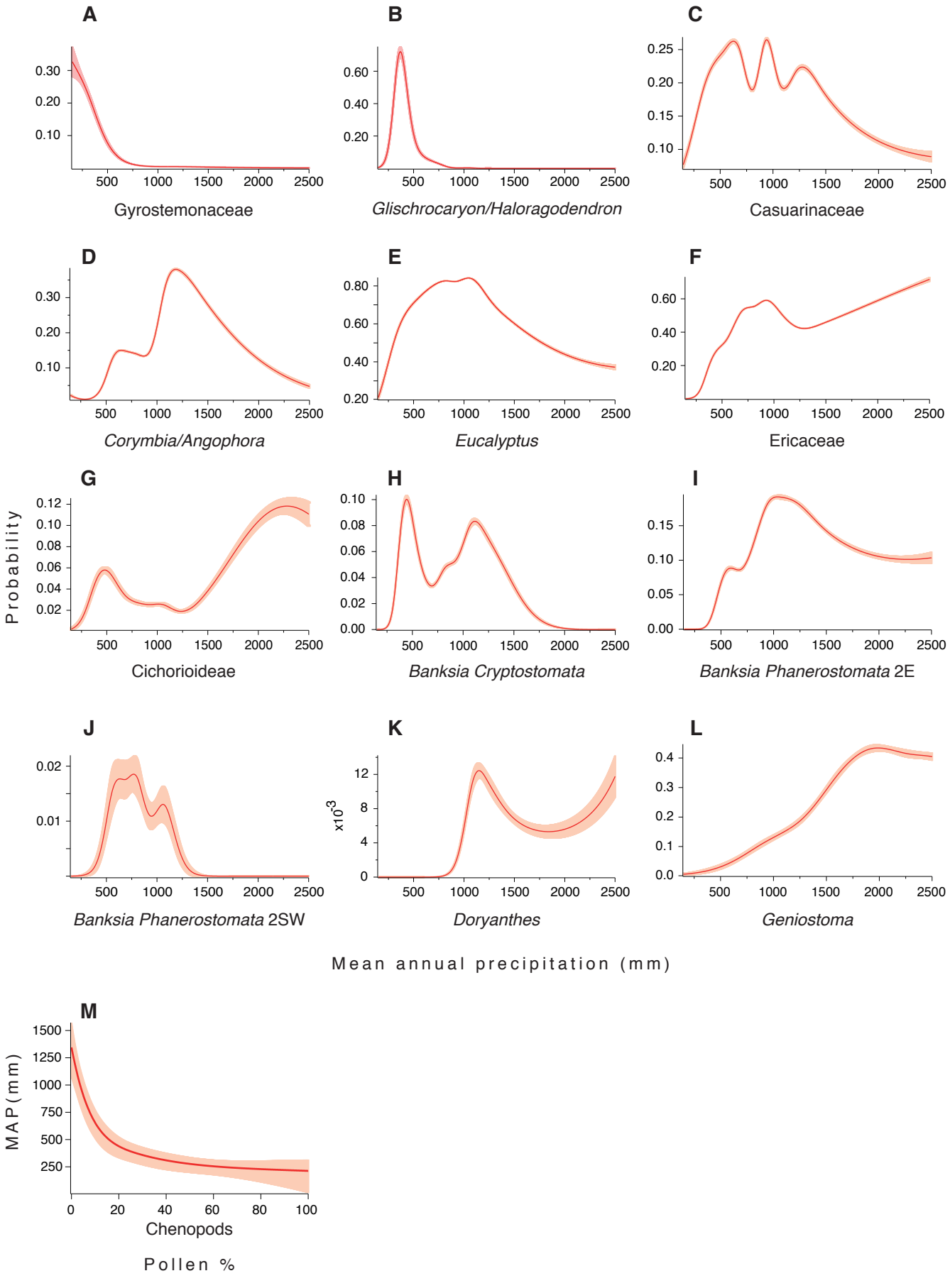
A
B
C
D
E
F
G
H
I
J
K
L
M
Gyrostemonaceae
Glischrocaryon/Haloragodendron
Casuarinaceae
Corymbia/Angophora
Eucalyptus
Ericaceae
Cichorioideae
Banksia Cryptostomata
Banksia Phanerostomata 2E
Banksia Phanerostomata 2SW
Doryanthes
Geniostoma
Probability
x10-3
Mean annual precipitation (mm)
MAP (mm)
Chenopods
Pollen %

Figure S4

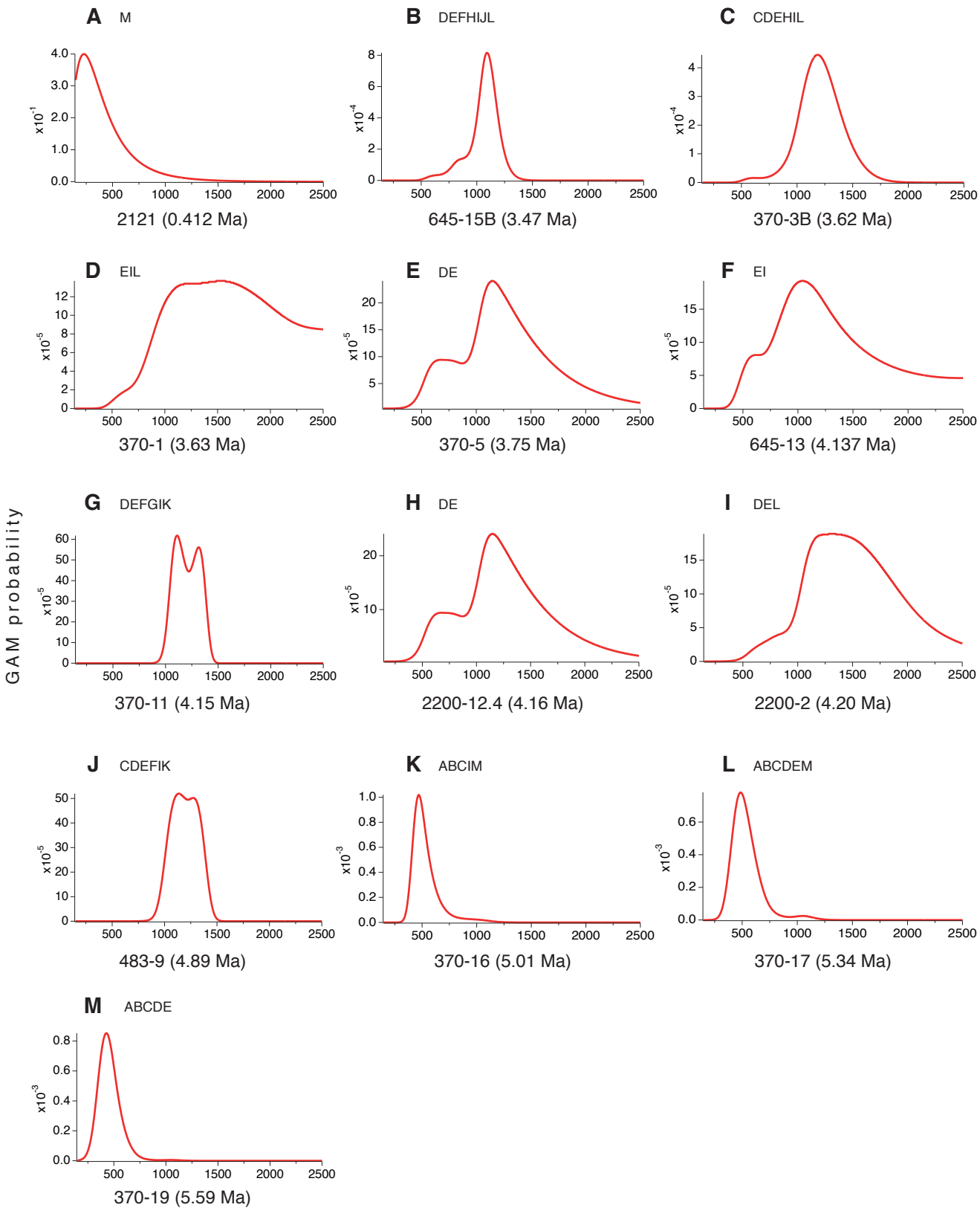
A M
2121 (0.412 Ma)
B DEFHIJL
645-15B (3.47 Ma)
C CDEHIL
370-3B (3.62 Ma)
D EIL
370-1 (3.63 Ma)
E DE
370-5 (3.75 Ma)
F EI
645-13 (4.137 Ma)
G DEFGIK
370-11 (4.15 Ma)
H DE
2200-12.4 (4.16 Ma)
I DEL
2200-2 (4.20 Ma)
J CDEFIK
483-9 (4.89 Ma)
K ABCIM
370-16 (5.01 Ma)
L ABCDEM
370-17 (5.34 Ma)
M ABCDE
370-19 (5.59 Ma)
GAM probability
Mean annual precipitation (mm)

Figure S5

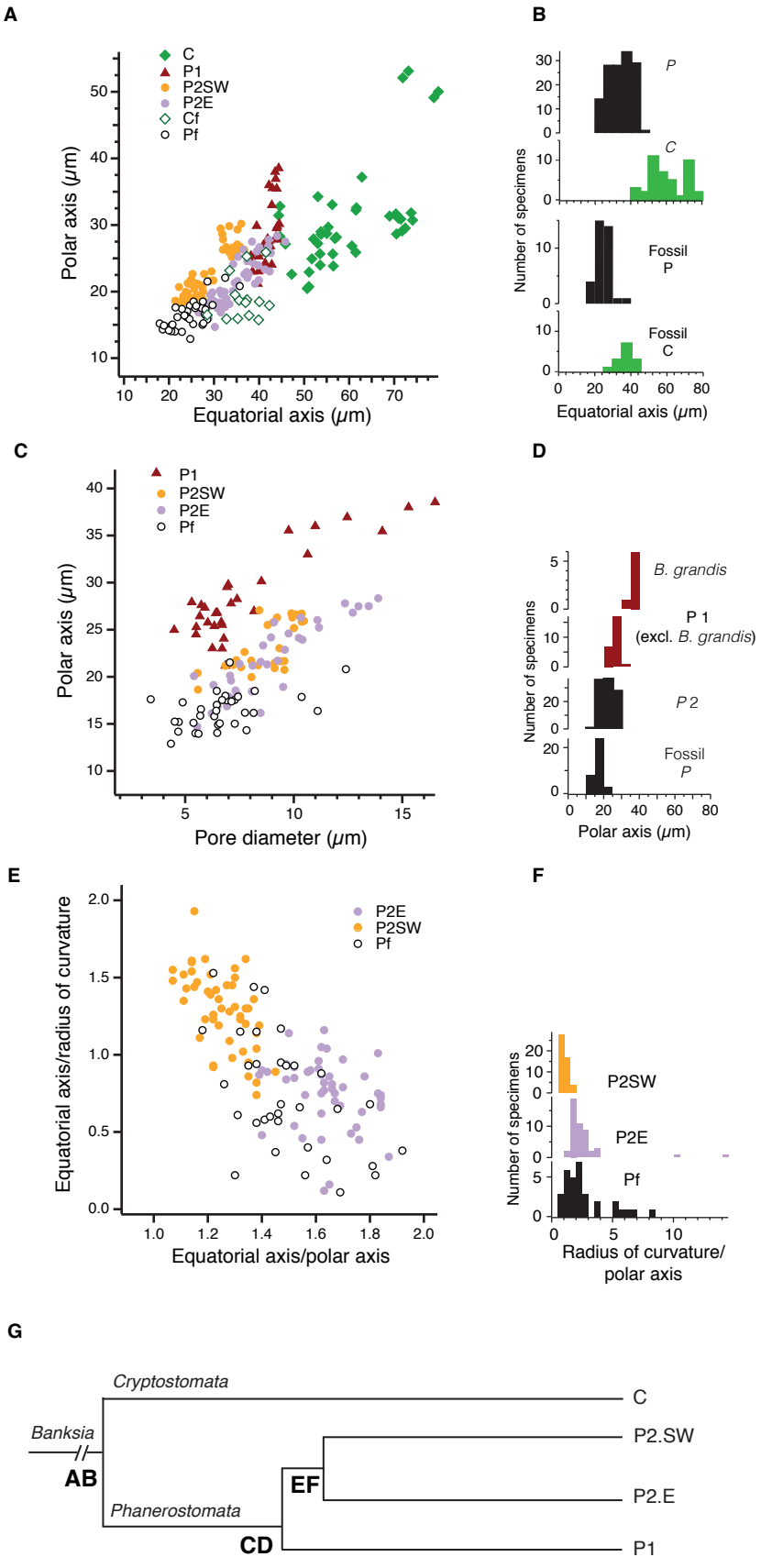
A
C
P1
P2SW
P2E
Cf
Pf
Polar axis (μm)
Equatorial axis (μm)
B
P
C
Fossil P
Fossil C
Number of specimens
Equatorial axis (μm)
C
P1
P2SW
P2E
Pf
Polar axis (μm)
Pore diameter (μm)
D
B. grandis
P 1 (excl. B. grandis)
P 2
Fossil P
Number of specimens
Polar axis (μm)
E
P2E
P2SW
Pf
Equatorial axis/radius of curvature
Equatorial axis/polar axis
F
P2SW
P2E
Pf
Number of specimens
Radius of curvature/ polar axis
G
Cryptostomata
Banksia
AB
Phanerostomata
EF
CD
C
P2.SW
P2.E
P1

Figure S6